



1 Sensitivity of Andean Glaciers to ice-flow parameters in the Parallel 2 Ice Sheet Model

3 Ethan Lee¹, Jeremy C. Ely¹, Sarah L. Bradley¹, Tamsin L. Edwards², Bethan J. Davies³

4 ¹ School of Geography and Planning, University of Sheffield, Sheffield, S3 7ND, UK

5 ² Department of Geography, King's College London, London, WC2B 4BG, UK

6 ³ School of Geography, Politics and Sociology, Newcastle University, Newcastle upon Tyne, NE1 7RU, UK

7 *Correspondence to:* Ethan Lee (ethan.lee@sheffield.ac.uk)

8

9 **Abstract.** Mountain glaciers are losing mass rapidly due to anthropogenic climate change. Projections of glacier evolution
10 across the Andes under different warming scenarios have primarily been as part of global scale modelling frameworks, rather
11 than dedicated, regionally optimised, simulations. These global-scale models use simplifications of ice flow physics that may
12 be unsuitable for steep topography, such as that which occurs at mountain valley glaciers. More complex models are available,
13 but with that complexity comes further sources of uncertainty. Here, we assess the sensitivity of the Parallel Ice Sheet Model
14 to ice-flow parameters influencing the ice rheology and subglacial sliding characteristics. We find that the resistance of
15 subglacial material has the most impact on modelled ice outputs (e.g., ice volume), followed by the exponent which relates
16 basal shear stress to sliding, and the threshold velocity at which sliding occurs. The ice-flow rheology enhancement factors,
17 the rate of subglacial water decay, and the maximum water thickness within a presumed subglacial drainage network, can
18 either cause minor variations, or no effect at all, on ice outputs. Our study informs what parameters can potentially be negated
19 in future parameter ensemble tests and provides direction on where further investigation is needed.

20

21 1 Introduction

22 Andean glaciers are a critical part of the region's water tower system (Immerzeel et al., 2020), particularly during droughts
23 (Drenkhan et al., 2015) and in upland rural areas (Buytaert et al., 2017; Rabatel et al., 2013). However, they are losing mass
24 rapidly (Dussaillant et al., 2019), placing stress on water resources, and contributing to sea level rise. Continued global
25 warming, intensified by regional elevation-dependent warming (Byrne et al., 2024; Pepin et al., 2015), and changing
26 precipitation regimes (Cai et al., 2020; Masiokas et al., 2020; Potter et al., 2023) heighten the need for accurate glacier
27 projections to inform water management and sea level rise assessments.

28 Global-scale models of glaciers and ice caps (i.e., all land-based ice not stored in ice sheets) predict continued ice loss through
29 to 2100 (Hock et al., 2019; Hugonnet et al., 2021; Rounce et al., 2020). While long-term sea level rise will be dominated by
30 the Greenland and Antarctic Ice Sheets (Goelzer et al., 2020; Seroussi et al., 2024), glaciers and ice caps may contribute up to
31 0.35m of sea level rise by 2100 (Edwards et al., 2021; Hock et al., 2019; Marzeion et al., 2020). These global-scale experiments



32 are designed to capture the envelope of plausible sea level rise contributions from glaciers under different emission scenarios
33 (Fox-Kemper et al., 2023). However, global and regional scale projections of mountain glacier change are not only needed for
34 sea level rise, but also for management of changing water resources, mountain glacier hazards, resources for tourism and
35 recreation, and for ecological and biodiversity management.

36 Glacier models used in intercomparison efforts such as GlacierMIP (Hock et al., 2019; Marzeion et al., 2020; Rounce et al.,
37 2023) provide insight at global and regional scales (Zekollari et al., 2025). However, their use may be limited for planning
38 local resource management and mitigations due to: i) simplified ice-flow physics unsuited to steep topography (Egholm et al.,
39 2011); ii) reliance on downscaled global climate models (GCMs), which often poorly capture mountain climate (Núñez Mejía
40 et al., 2023); and iii) simplified mass balance schemes, often reduced to positive degree-day models (PDD; Bolibar et al.,
41 2022).

42 Here we attempt to address the first issue, by using a complex ice sheet model to assess uncertainties in the parameterisation
43 of glacier ice flow physics in areas of steep mountain topography. We use the Parallel Ice Sheet Model (PISM; Winkelmann
44 et al., 2011), a thermomechanically coupled shallow-ice/shallow-shelf model commonly applied to both ice sheets (Johnson
45 et al., 2023; Payne et al., 2021; Seroussi et al., 2024) and mountain glaciers (e.g., Candaş et al., 2020; Martin et al., 2022;
46 Žebre et al., 2021). PISM incorporates subglacial hydrology and basal sediment (till) deformation (Albrecht et al., 2020;
47 Winkelmann et al., 2011), but the added complexity increases the number of uncertain parameters. Perturbed parameter
48 ensembles are generally used to explore this type of uncertainty (e.g., Berdahl et al., 2021; Roe and Baker, 2014), however,
49 the number of simulations tends to increase with the number of parameters used, leading to significant computation for
50 computationally expensive models (Archer, 2024; Rougier, 2015). Therefore, a useful precursor to such efforts is a targeted
51 sensitivity analysis to identify which parameters meaningfully influence model outputs. This can aid in excluding parameters
52 from a full ensemble design that show low control over model output, saving computation resources and time.

53 The aim of this study is to assess the sensitivity of modelled Andean glaciers to ice-flow parameters within PISM. We explore
54 this parameter space through a suite of steady-state univariate and multivariate sensitivity experiments across selected Andean
55 glacier catchments. We focus solely on parameters controlling internal ice deformation and glacier-bed interactions.

56

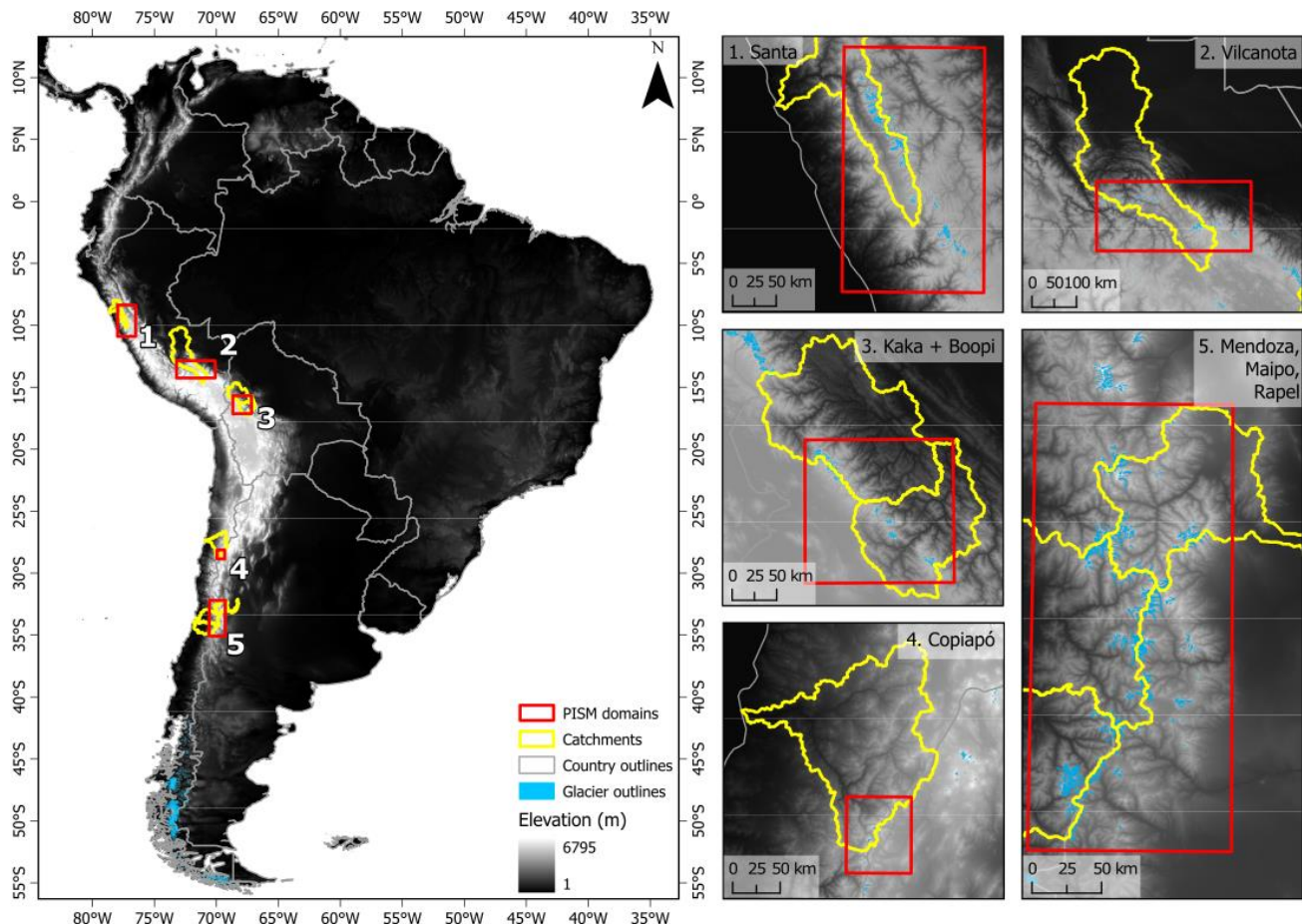
57 2 Study area

58 Mountain glaciers and ice caps in the Andes span 68° of latitude, from 12°N in Columbia, to 56°S in Chile and Argentina.
59 Projections over Andean glaciers show they are likely to become significantly smaller, or entirely lost, in the future due to
60 climatic warming (e.g., Zekollari et al., 2025). Rounce et al. (2023) estimates mass losses by 2100 for the Low Latitudes (RGI
61 16) of $69 \pm 25\%$ to $98 \pm 2\%$, and for the Southern Latitudes (RGI 17) $38 \pm 15\%$ to $68 \pm 20\%$ for the low and very high emission



62 scenarios RCP2.6 (mean projected global warming +1.6°C by 2100) and RCP8.5 (+4.3°C), respectively. Under the more recent
63 SSP scenarios, Rounce et al., (2023) projected slightly higher losses: from $76 \pm 18\%$ to $99 \pm 3\%$ in the Low Latitudes, and
64 from $49 \pm 19\%$ to $74 \pm 22\%$ in the Southern Andes, under SSP1-2.6 (+1.8°C) and SSP5-8.5 (+4.4°C), respectively. More
65 recently, Zekollari et al. (2025) detailing the committed loss of glaciers after equilibrating with global warming estimates of
66 +1.5°C and +4.0°C, the Southern Andes would lose a mean of 45% and 79% of their mass, and the Low Latitudes a mean of
67 46% and 96% of their mass respectively. Regionally specific in Peru, Drenkhan et al. (2015) projects area losses between
68 40.7% and 44.9% by 2060 under RCP2.6, and between 41.4% and 92.7% by 2100 under RCP8.5.

69 The five PISM model domains used in this study encompass the mountain glaciers in the 1) Santa, 2) Vilcanota, 3) Kaka and
70 Boopi, 4) Copiapó and 5) Mendoza, Maipo, and Rapel hydrological catchments (Fig. 1). The glaciers in these hydrological
71 catchments are particularly important for their role as meltwater sources for downstream populations (Masiokas et al., 2020;
72 Vuille et al., 2008). The chosen domains cover three different climatological zones: domains 1, 2, and 3 are within the tropical
73 Andes, with a diurnal temperature variation that outweighs the annual temperature variation. This leads to glaciers being
74 sensitive to changes in precipitation that impact the presence and distribution of snowfall across the glacier surface (Hardy et
75 al., 1998; Kaser, 1999). Domain 4 lies within the desert Andes, with high snowline altitudes. This arid climate has short
76 snowfall events that cause glaciers to lose mass primarily through sublimation (Fyffe et al., 2021; Masiokas et al., 2016).
77 Lastly, domain 5 comprises three adjacent mountain hydrological catchments within the wet Andes that are sensitive to
78 temperature changes, due to receiving substantial snowfall during the winter months (Masiokas et al., 2016), while the presence
79 of glacial lakes enhances mass loss through calving and proglacial lake-driven melting (Wilson et al., 2018).



80
81 **Figure 1: Chosen hydrological catchments and the five PISM domains across the South American Andean Mountains used in this**
82 **sensitivity analysis. Red outlines show the model domains, focused on glacierized areas within each hydrological catchment.**
83 **Hydrological catchment boundaries are from HydroSHEDS (Lehner et al., 2008).**

84 The Andes have been the focus of numerous studies examining glacier extent changes in response to both centennial (e.g.,
85 Carrivick et al., 2024; Emmer et al., 2021) and decadal scales (e.g., Dussaillant et al., 2019; Taylor et al., 2022). Global-scale
86 studies using simplified two-dimensional flowline models (e.g., OGGM; Maussion et al., 2019) have modelled individual
87 Andean glaciers as part of broader global modelling frameworks, which apply uniform modelling frameworks across diverse
88 climatic and topographic regimes. Although these global frameworks can assimilate regional climate data, they do not
89 specifically optimise for Andean glacier dynamics and are unable to account for highly heterogeneous climatic regimes such as
90 those of Andean glaciers. However, regional-scale glacier modelling specific to the Andes remains limited. Most physically
91 based modelling efforts have been concentrated on the Patagonian Icefields, a setting distinct from the rest of the Andes, while
92 other studies are primarily focused on modelling from the Last Glacial Maximum to present (e.g., Cuzzzone et al., 2024; Martin
93 et al., 2022; Wolff et al., 2023; Yan et al., 2022). To date, only one study has focused in detail on modelling Andean Mountain
94 glaciers outside Patagonia, assessing their response to climate extremes, however, this study is restricted to just two glaciers



95 (Richardson et al., 2024). Consequently, parameter choices and process understanding for physically based modelling of
96 Andean glaciers remain poorly constrained.

97

98 3 Materials and methods

99 3.1 Parallel Ice Sheet Model

100 Here, we used the Parallel Ice Sheet Model (PISM v2.1) (Winkelmann et al., 2011) to conduct our numerical modelling. PISM
101 is an open-source, three-dimensional, thermomechanically coupled, hybrid shallow ice, shallow shelf, approximation ice sheet
102 numerical model. The parameter combinations of PISM can be calibrated to represent localised climate and glaciological
103 conditions when sufficient observational constraints (e.g., mass balance data, surface velocity, past glacier extents) are known.
104 Otherwise, default parameter values, which have primarily been tuned for the Greenland Ice Sheet, are set automatically if not
105 specified. Key parameters we have chosen to change here are mentioned throughout the following sections and in [Table 1](#).

106 **Table 1: Chosen glaciological model parameters for sensitivity analysis within PISM. Letters on the leftmost edge of the table**
107 **correspond to the component letter within PISM that the chosen parameters cover, which is also explained in the main text. All**
108 **other parameters not mentioned within this table are left at their default values, which can be found in PISM's Configuration**
109 **Parameters online manual (<https://www.pism.io/docs/manual/parameters/index.html>).**

| Parameter | Default | Min | Max | Description |
|-----------|---------------------|------|------|-------------|
| E | E_{SIA} / E_{SSA} | 1 | 0.2 | 20 - |
| T | C | 1 | 0.1 | 12 mm/a |
| | W_{tilt}^{max} | 2 | 0.1 | 10 m |
| | ϕ | 30 | 5 | 45 ° |
| S | q | 0.25 | 0.05 | 0.95 - |
| | $U_{threshold}$ | 100 | 20 | 200 m/a |

110

111 3.1.1 Enhancement Factors (E Component)



112 We used PISM's hybrid shallow ice shallow shelf approximation (hybrid SIA+SSA). This is the combination of the shallow-
113 ice (SIA; Hutter, 1983; Mangeney and Califano, 1998) and shallow-shelf approximations (SSA; Bueler and Brown, 2009;
114 Weis et al., 1999), enabling PISM to represent both the vertical deformation and longitudinal stretching of the ice, along with
115 basal sliding. This hybrid SIA+SSA has been applied in other valley-based glacial systems (Candaş et al., 2020; Golledge et
116 al., 2012; Martin et al., 2022; Seguinot et al., 2018).

117 The stress balance, and the resulting rate of ice deformation ($\dot{\epsilon}$), is described by the Glen-Paterson-Budd-Lliboutry-Duval flow
118 law (Lliboutry and Duval, 1985). This is the default enthalpy-based flow law within PISM, shown in Eq. 1,

$$\dot{\epsilon}_{ij} = EA(T, \omega)\tau^{n-1}\tau_{ij}, \quad (1)$$

119 where E is the enhancement factor, A is the ice softness, T is the ice temperature, ω is the liquid water fraction, τ is the stress
120 imposed on the ice, and n is the Glen's flow law exponent. E is implemented for both the SIA and SSA.

121 For the sensitivity tests, we changed the parameterisation of E for both the SIA and SSA. Many studies have varied E_{SIA} with
122 values between 1 and 6 (Candaş et al., 2020; Ely et al., 2024; Johnson et al., 2023; Zinck and Grinsted, 2022), and E_{SSA} between
123 0 and 1.5 (Martin et al., 2022; Seguinot et al., 2018; Yan et al., 2023). We varied both E_{SIA} and E_{SSA} at the same time between
124 0.2 and 20 (see Table 1).

125

126 3.1.2 Subglacial properties (T Component)

127 In PISM, the subglacial hydrology and sliding scheme was originally developed for ice-sheet contexts and conceptualises the
128 bed as a deformable layer, to represent subglacial 'till' or sediment, that can store water and influence basal resistance. The
129 extent to which this subglacial sediment is under ice sheets is unknown, which is also the case for Andean glaciers, although
130 thick layers of sediment are present in glacier forefields. However, the formulation for glacier sliding and hydrology does not
131 require sediment to be present everywhere beneath the glacier. The effective pressure and sliding behaviour can equally
132 represent hard-bedded conditions, where subglacial water storage may occur within bedrock cavities rather than within
133 sediments. To note, while we use the term 'till' throughout this study for consistency with PISM terminology and previous
134 studies, it should not be interpreted as implying continuous sediment cover beneath Andean glaciers.

135 The yield stress of the basal material (τ_c) in PISM is calculated using the Mohr-Coulomb criterion, which incorporates the till
136 friction angle till friction angle (ϕ), a parameter influenced by the underlying bed geology (Albrecht et al., 2020; Cuffey and
137 Paterson, 2010). This relationship is partly governed by PISM's subglacial hydrology model. The Mohr-Coulomb criterion
138 used to compute yield stress is given in Eq. 2,



$$\tau_c = c_0 + (\tan\phi)N_{till} \quad (2)$$

139

140 Where c_0 is the till cohesion that uses a default value of 0 (Schoof, 2006), and N_{till} is the effective pressure at the base of the
 141 ice within the till layer. For every domain we applied a spatially uniform ϕ . Previously used values of ϕ have generally been
 142 within ranges of values 5-45°, derived from lab-based experiments of different till types (Cuffey and Paterson, 2010; Koloski
 143 et al., 1989). The default value in PISM is 30°, while in the sensitivity tests, we varied ϕ between 5° and 45° (see Table 1).

144 Within Equation 2, N_{till} is determined in part by the hydrology beneath the ice. The hydrological model used here is a non-
 145 conserving model (Tulaczyk et al., 2000). This does not allow the conservation of any water above an assigned till water
 146 thickness (W_{till}^{max}). The thickness of the water layer stored within the till is determined by Eq. 3,

$$\frac{\partial W_{till}}{\partial t} = \frac{m}{\rho_w} - C \quad (3)$$

147 Where m is the basal melt rate, ρ_w is the density of fresh water (1000 kg m³), and C is the till water decay rate that denotes
 148 how fast water is evacuated from the till water (Albrecht et al., 2020; Flowers, 2015). At all times within the model, $0 \leq$
 149 $W_{till} \leq W_{till}^{max}$ must be satisfied, with any water above W_{till}^{max} being removed.

150 C and W_{till}^{max} are tested in our sensitivity analysis through the T Component. The till water decay rate is varied between 0.1
 151 and 12 mm/a, while the maximum till water thickness is varied between 0.1 and 10 m (see Table 1).

152

153 3.1.3 Basal sliding (S Component)

154 In PISM, basal sliding is represented by relating the basal shear stress (τ_b) to both the ice velocity (u) and effective pressure
 155 (N). A velocity threshold ($u_{threshold}$) marks when τ_b equals the yield stress (τ_c), and therefore when sliding occurs (Cuffey
 156 and Paterson, 2010). By default, within PISM we used the Zoet and Iverson (2020) slip law, which introduces a regularisation
 157 term that enables a smooth transition between the viscous-style Weertman sliding (Weertman, 1957), and the Coulomb-plastic
 158 behaviours (Aschwanden et al., 2013), without needing prior knowledge of bed type. The Zoet and Iverson (2020) slip law is
 159 expressed in PISM by Eq. 4,

$$\tau_b = -\tau_c \frac{u}{(|u|+u_{threshold})^q|u|^{1-q}}, \quad (4)$$

160

161 Zoet and Iverson (2020) in their equation parameterise $q = 1/m$ where $m = 5$, whereas PISM's default value of q is 0.25 (or
 162 where $m = 4$). While the Zoet and Iverson (2020) slip law is relatively new in PISM, being introduced in v2.0, few PISM



163 studies have utilised it. Those modelling efforts that have used the Zoet and Iverson (2020) slip law, (e.g., the Community Ice
164 Sheet Model or CESM; Lipscomb et al., 2019), have varied it between narrow ranges. These have been at 0.2 (Khan et al.,
165 2022; Moreno-Parada et al., 2023), 0.23 (Maier et al., 2022), or 0.33 (van den Akker et al., 2025; Hoffman et al., 2022; Joughin
166 et al., 2024).

167 Within our sensitivity analysis, q and $u_{threshold}$, were tested through the S component. We varied q from 0.05 to 0.95 to
168 maximise the coverage of potential parametrisations of q to the extremes. We also varied $u_{threshold}$, a parameter that has seen
169 some variation in other modelling studies (Bevan et al., 2023; Martin et al., 2022; Seguinot et al., 2014, 2018). We varied the
170 $u_{threshold}$ between 20 and 200 m/a (see [Table 1](#)).

171

172 3.1.4 Surface mass balance

173 We used PISM's default positive degree day (PDD) temperature-index scheme (Calov and Greve, 2005) to generate ice within
174 the domains. This required monthly mean air temperature and yearly precipitation (see Sect. 3.3). Within the PDD scheme,
175 there is stochastic 'white noise' to simulate additional undetermined daily variability, as well as a daily temperature standard
176 deviation that is set by default at 5°C (Winkelmann et al., 2011). These can cause minor fluctuations in the climate, and thereby
177 in the ice extent even under steady state conditions. We forced the model with a constant present-day climate (see Sect. 3.3),
178 to allow glacial ice to reach steady state with its surrounding climate. Parameters that affect the PDD model component of
179 PISM, such as degree day factors, were kept at their default values and not varied within this study due to these values being
180 unknown and this study only being concerned with the internal ice model parameters.

181

182 3.2 Model setup and parameter sensitivity analysis

183 The five model domains simulated by PISM are shown in [Fig. 1](#). Each domain had a 100 m horizontal grid resolution
184 (dimensions in [Table 2](#)), with 50 vertical ice layers (quadratic spacing) and 10 bedrock layers. This resolution resolves the
185 topography and flow characteristics while maintaining feasible wall-clock run times. All domains were initialised without
186 prescribed ice thicknesses and run to steady state (~1,500 model years) under constant climate forcing (see Section 3.2).

187 **Table 2: PISM study domains, detailed with their grid x, y sizes at 100 m resolution, and the domain area along with the RGIv7 ice**
188 **area of each domain. The location of each domain, and the hydrological catchments they partially cover, are shown in [Fig. 1](#).**

| Domain | x | y | Area (km ²) | Ice Area (km ²) |
|----------------------------|------|------|-------------------------|-----------------------------|
| 1) Santa, Peru | 1600 | 2800 | 44,800 | 607 |
| 2) Vilcanota, Peru | 3400 | 1600 | 54,400 | 515 |
| 3) Kaka and Boopi, Bolivia | 1600 | 1600 | 25,600 | 240 |
| 4) Copiapó, Chile | 600 | 800 | 4,800 | 35 |



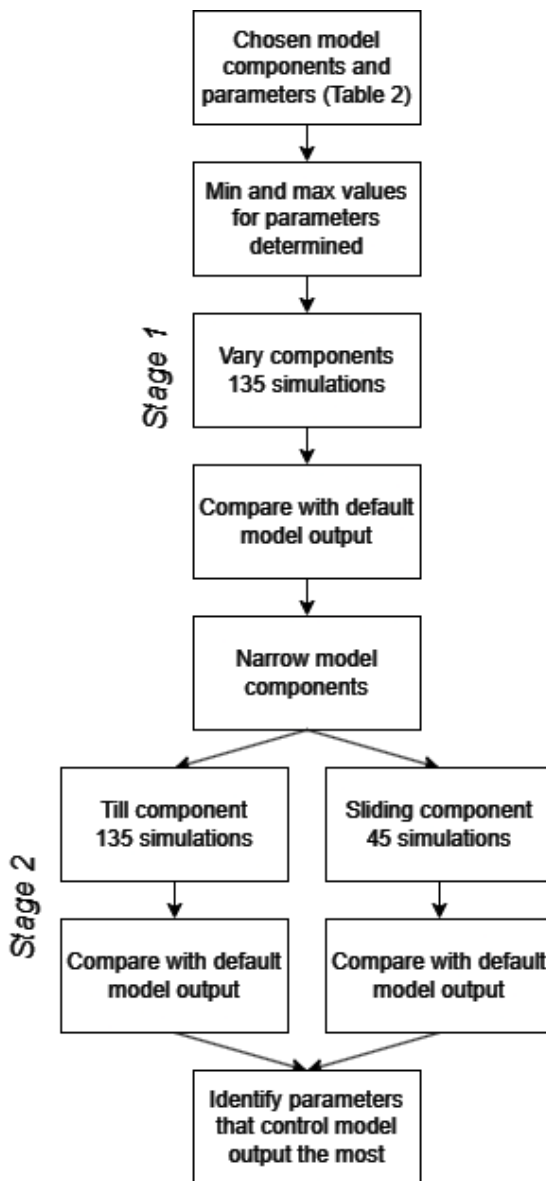
189 5) Mendoza, Maipo, and Rapel, Chile 1200 3600 43,200 1,303

189

190 Our sensitivity analysis focused on internal ice-flow parameters. These parameters define the physical properties and processes
191 governing ice behaviour, such as the shallow ice, and shallow shelf approximation (SIA/SSA) flow enhancement factor, basal
192 sliding, and subglacial mechanics. We targeted parameters that: (i) have shown substantial influence on glacier modelling in
193 previous studies; (ii) are commonly tested in sensitivity analyses; and (iii) remain poorly constrained by observations or past
194 modelling.

195 The analysis followed a two-stage approach (Fig. 2) to enable efficient identification of components that exert the greatest
196 control over model outputs. This coarse screening (Stage 1) allowed subsequent parameter-specific tests (stage 2) to focus only
197 on the most sensitive components governing ice flow. This aim of this is to reduce the dimensionality of the analysis and the
198 computational cost of future ensemble experiments. This two-stage approach can be used by other sensitivity studies to
199 facilitate more efficient sampling of key aspects of the model in question that causes the most effect on chosen outputs.

200 In stage 1 (135 model simulations: 27 per domain), we group individual parameters into components impacting three key ice-
201 flow processes: enhancement factors (E), basal sliding (S), and subglacial properties (T). Parameter values spanned both
202 commonly used and extended ranges to capture a broad spectrum of glacier responses. Each component was perturbed between
203 its chosen minimum, maximum, and default values (Table 1), first individually (with all other components fixed at default
204 values) and then simultaneously, to generate the ensemble design for each domain. Components that showed negligible
205 influence on outputs were discarded from further analysis.



206

207 **Figure 2: Flow diagram of sensitivity experiment design detailing the staged approach.**

208 Stage 2 (180 model simulations: 36 per domain) comprised a detailed within-component analysis of only those components
209 identified in Stage 1 as influential. Here, every individual parameter was perturbed one-at-time across their defined value
210 ranges (min, max, default; Table 1), followed by simultaneous perturbation of all parameters within that component, rather
211 than grouping them by component as in Stage 1. Parameter in each figure and table corresponds to a shortened name presented
212 here; enhancement factor (E), till water decay rate (C), maximum till water thicknesses (T_m or W_{till}^{max}), till friction angle (Phi
213 or ϕ), sliding exponent (q), velocity threshold (U_{th} or $U_{threshold}$).



214 Model outputs, of ice volume, ice thickness, and basal velocity, were compared against the baseline simulation using the
215 default values for all parameters. To quantify influence, results were averaged over the domain and Pearson correlation
216 coefficients were calculated between these and the parameter values, along with p-values to assess statistical significance of
217 their effect. This approach provided both a ranking of parameter sensitivity and an assessment of the robustness of their effects.

218

219 **3.3 Boundary conditions data**

220 Topography is a key initial condition within PISM. We used the ALOS 30 m DEM (Tadono et al., 2014), due to its accuracy
221 over complex mountainous terrain (Talchabhadel et al., 2021), resampled to 100 m using a bilinear interpolation. Basal
222 topography was derived by subtracting present-day ice thicknesses of Millan et al. (2022) from the ALOS DEM. Ice thickness
223 was not directly inputted to the model for the sensitivity experiments.

224 Geothermal heat flux is required to define and apply the temperature of the bed to the base of the ice. We used Davies (2013)
225 which uses the relationship between basal heat flux to geology on a $2^\circ \times 2^\circ$ global grid. Due to the lack of regional specific
226 geothermal heat flux estimates within our study areas and the coarse nature of the dataset, for each domain we assigned a
227 single value based on the value from the grid cell containing the most glacial ice.

228 Climate input is required for the PISM PDD scheme. For our present-day climate, we used the WorldClim 2.1 data (Fick and
229 Hijmans, 2017). WorldClim 2.1 is a gridded climate data for the years 1970-2000 collected from weather stations here we use
230 the average air temperature (K) and average total annual precipitation (mm yr⁻¹), resampled from a grid resolution of ~900 m
231 to 100 m bilinearly. Due to air temperatures from WorldClim being based on the 30 arc second SRTM DEM, it underestimates
232 temperatures across mountain peaks. To remedy this, we applied a lapse-rate correction of 6.5°C/km based on elevation
233 differences between the WorldClim SRTM and resampled ALOS DEMs. Erroneous adjustments due to DEM artefacts were
234 removed and interpolated across linearly. Ultimately, we are not concerned about the size and shape of the glaciers produced.
235 The role of the climate forcing is simply to produce some ice from which we can understand model sensitivity from.

236

237 **4 Results and Discussion**

238 Here, we outline results from the Stage 1 component sensitivity experiments for simulated volume change, then for the
239 subsequent Stage 2 parameter sensitivity experiments, for all domains. Aggregated domain results are shown here, with
240 individual model simulation outputs (area, volume, and percentage changes for each domain) available in the Supplementary
241 Information (SI): component sensitivity (SI Tables 1–5), subglacial parameter sensitivity (SI Tables 6–10), and sliding
242 parameter sensitivity (SI Tables 11–15). Final time-slice outputs of ice thickness and ice velocities, along with their differences



243 with the default model simulation for their respective regions, are shown in SI Figures 1-40. Key examples of these are shown
244 throughout which are also shown in the SI for ease of comparison. As the ice area was largely unaffected by parameter changes,
245 they are shown in the sensitivity bar graphs for transparency, but only volume outputs are discussed in any detail, though area
246 is shown in some figures for comparison.

247

248 **4.1 Stage 1 – Model component sensitivity analysis**

249 Stage 1 is used to determine which model component influences the ice metrics the most, to guide the more detailed Stage 2
250 sensitivity analysis (Table 3; Fig. 3). We describe results for each component in turn here.

251 When varying E component parameters (Esia and Essa) were varied between their minimum and maximum values (Table 1)
252 resulted in ice volume changes of +5.4% to -9.9% from their defaults across all domains. These changes are reflected primarily
253 in ice thickness (Fig. 4), with maximum E values producing thinner ice (mean: -5.4%) and increased basal velocities (mean:
254 +4.8%), though the Vilcanota (#2) domain showed a velocity decrease of -11.9%. Minimum E values led to thicker ice (mean:
255 +3.2%) and reduced velocities (mean: -9.1%). Pearson correlations between E and ice volume were weak and statistically
256 insignificant across all domains ($p > 0.53$; Table 4).

257 **Table 3: Initial sensitivity analysis outputs detailing the default model simulation volume, and the maximum absolute percentage
258 changes for volume for each domain across the ensemble when components were varied between their maximum and minimum
259 values.**

| Domain | Volume (km ³) | | | |
|------------------------|---------------------------|------|------|--------------------|
| | Default | Max | Min | Max abs change (%) |
| Santa | 10.1 | 35.2 | 8.8 | 247.2 |
| Vilcanota | 3.1 | 5.1 | 2.5 | 64.1 |
| Kaka & Boopi | 2.2 | 3.8 | 1.6 | 71.8 |
| Copiapó | 1.1 | 1.9 | 0.6 | 68.5 |
| Mendoza, Maipo & Rapel | 17.6 | 34.4 | 12.1 | 95.2 |

260

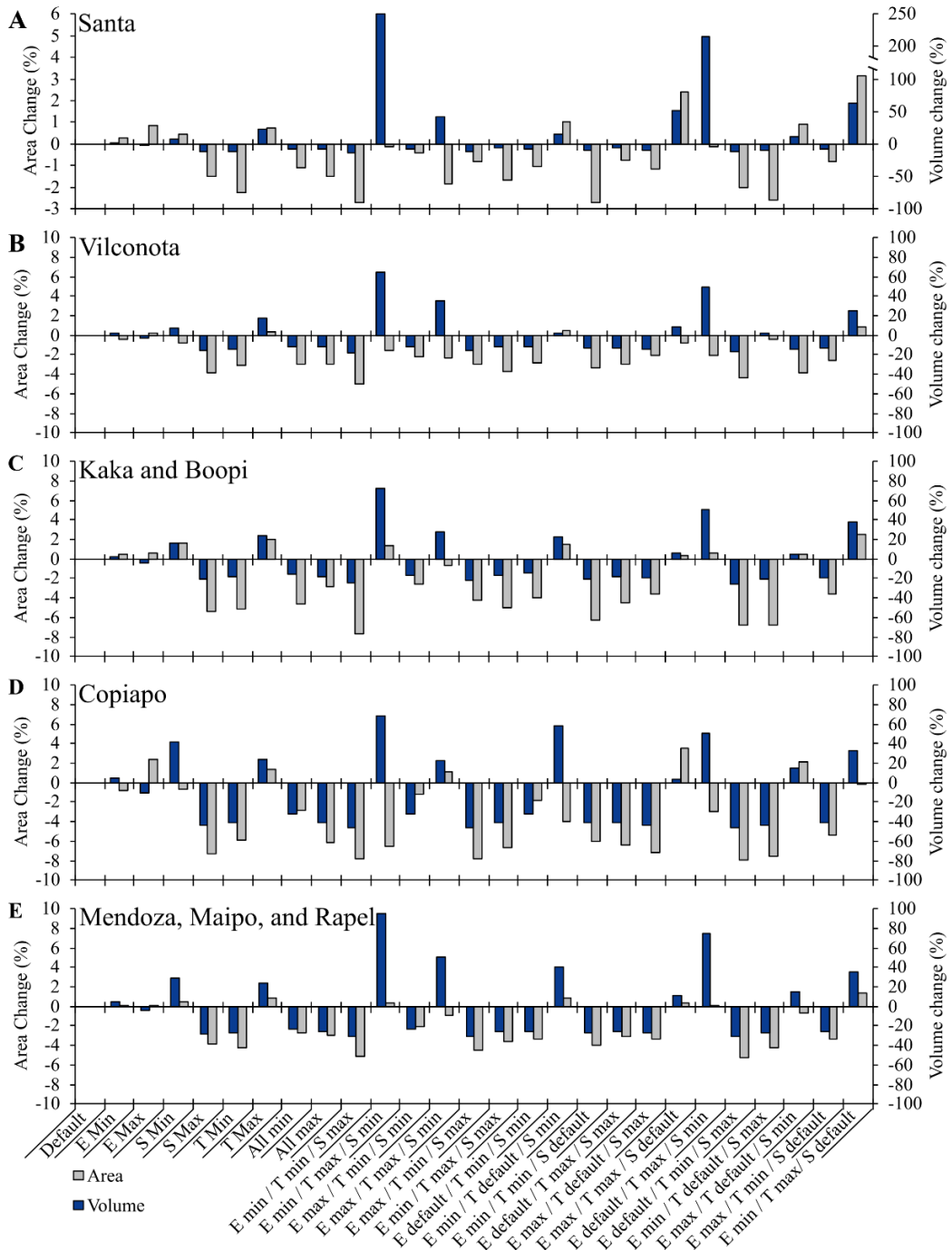
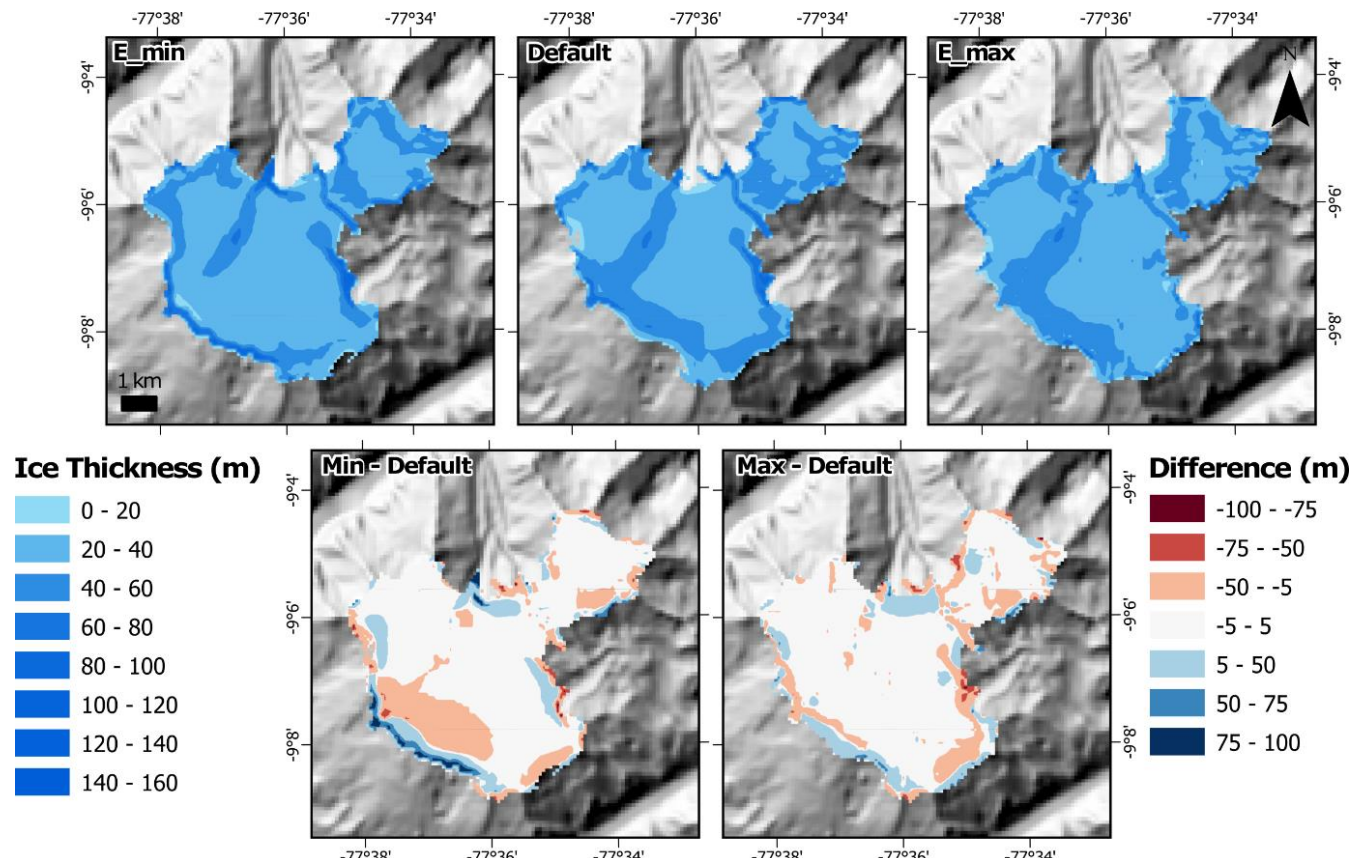


Figure 3: Initial sensitivity analysis detailing the area (grey) and volume (blue) absolute change percent due to changing all model component parameters together, for each of the five model domains. Blue and grey lines denote the default volume and area respectively for comparison. Component parameters are: E = enhancement factors, T = subglacial component, S = sliding component. See Fig. 1 for model domain locations. Note the break in y-axis for ice volume in A) detailing the significant increase in volume, above +200%.



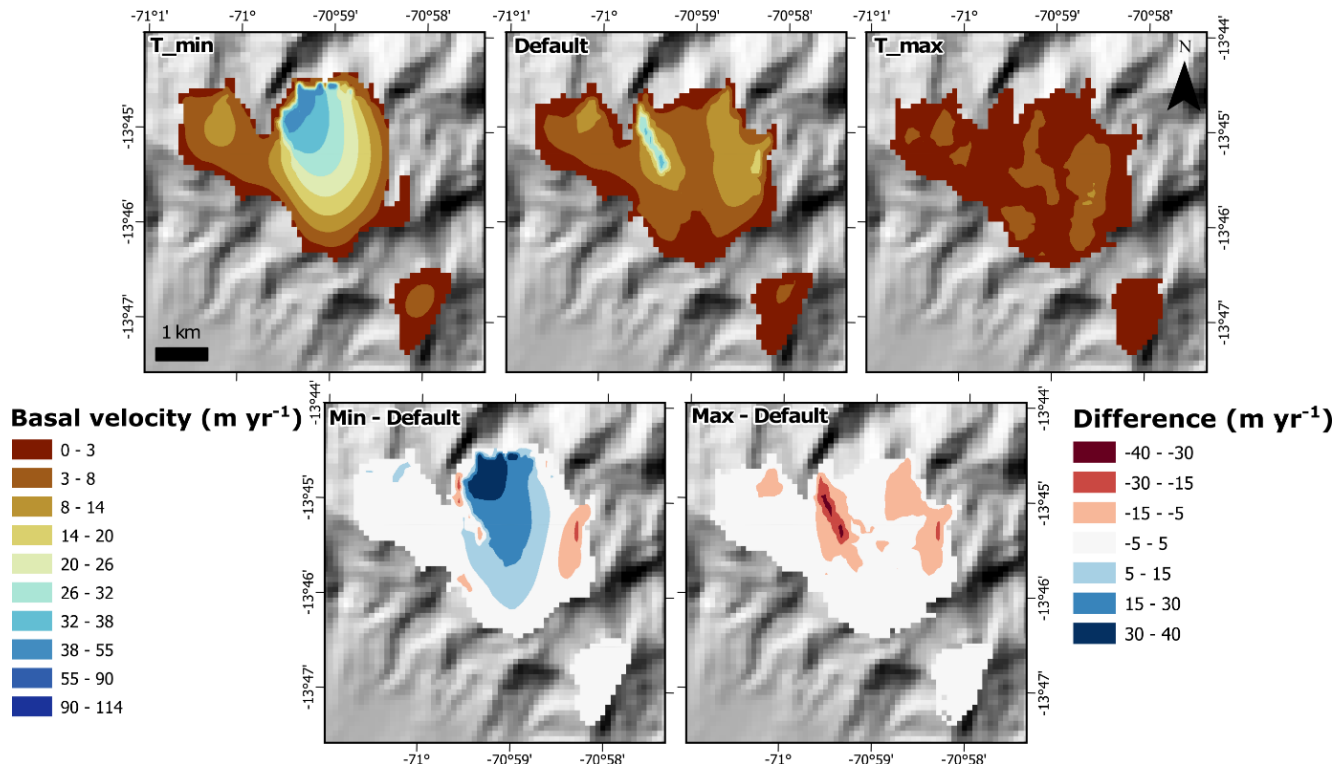
267
 268 **Figure 4:** Example of the influence of the enhancement factors on simulated ice thickness in the Santa (#1) domain (Huascarán Ice
 269 Cap). Additional examples are provided in the Supplementary Information. Ice peripheral differences in ice thickness arise from
 270 internal variability in the PDD model, despite a temperature standard deviation of 5°C. Parameter values for ‘max’ and ‘min’ are
 271 listed in Table 1.

272 Similar results - i.e., non-significant variations in modelled outputs - were reported using PISM in other mountain glacier
 273 settings (Candaş et al., 2020; Martin et al., 2022) and for ice caps (Schmidt et al., 2020). More substantial effects from the
 274 enhancement factors that impact ice rheology, have been observed in models of ice sheets (e.g., Lowry et al., 2020; Phipps et
 275 al., 2021; Pittard et al., 2022). Given the minimal impact of enhancement factors in this study, they were excluded from the
 276 Stage 2 sensitivity analysis.

277 When the T component parameters (subglacial water decay rate, maximum subglacial water thickness and bed friction angle)
 278 were varied between their minimum and maximum values (Fig. 3; Table 1) resulted in volume changes of -40.5% to +23.6%
 279 from their defaults across all domains. Minimum T parameter values increased basal sliding velocities substantially: up to
 280 +213.4% in the Copiapo (#4) domain (SI Fig. 12), a mean of +62.4% across all domains, leading to a mean ice thickness
 281 reduction of -20.9%. In contrast, maximum T parameter values reduced mean basal velocities by -49.2%, resulting in a mean
 282 thickness increase of +22.5% (Fig. 5). The resultant difference in the ice velocities and ice thicknesses can be seen in the shift

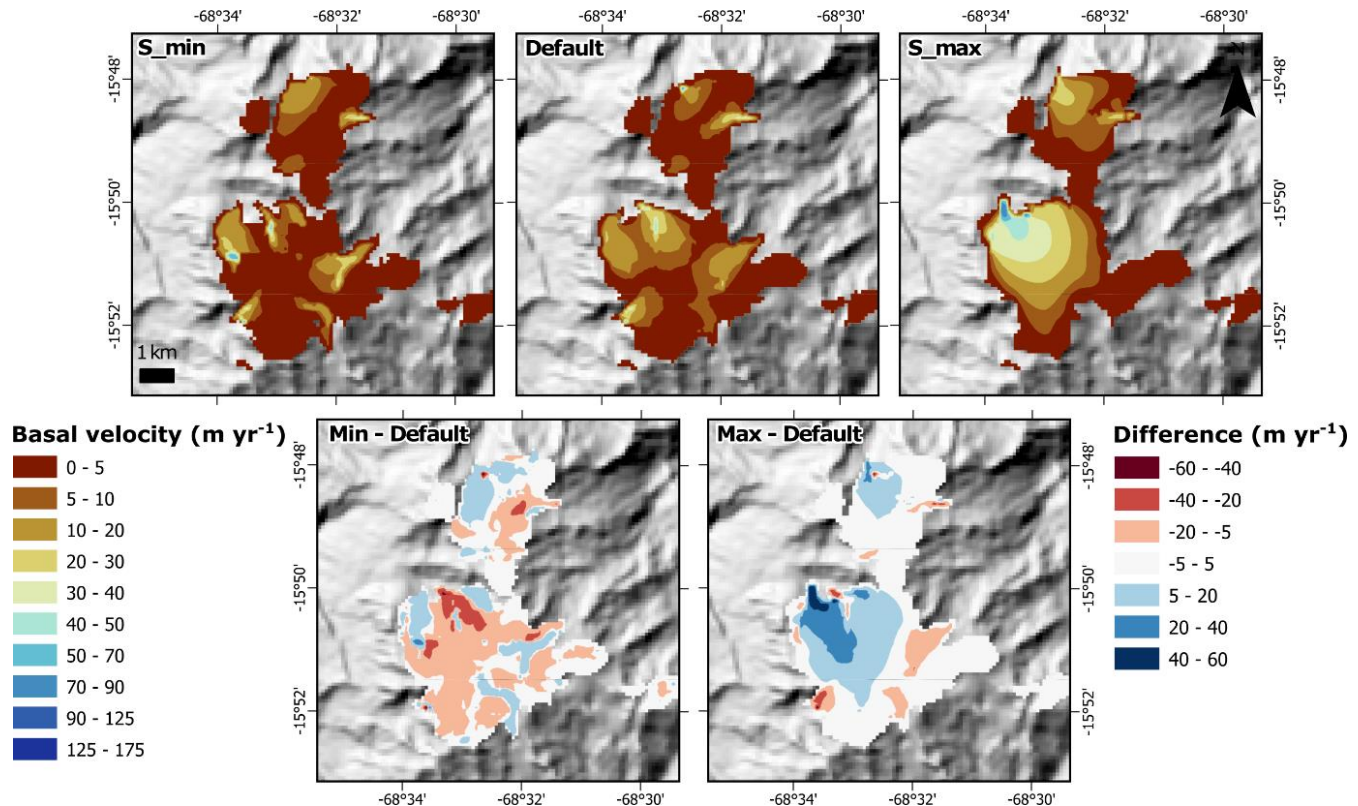


283 of the ice divide, being primarily constrained to the glacier valley, to being more diffuse with minimal T component values,
284 and being significant muted with maximum T component values.



285
286 **Figure 5: An example of the influence of the subglacial component chosen parameters on the output of ice basal velocity in Vilcanota**
287 (**#2**) domain (Quelccaya Ice Cap). Remaining examples are shown in the Supplementary Information. Increased values of the chosen
288 parameters generate reduced basal ice velocities, while decreasing values increase them. This can also lead to changes in ice divides
289 as seen in T_min, compared to T_max. Values that correspond to 'max' and 'min' parameter values are found in Table 1.

290 When the S component parameters (sliding exponent and velocity threshold) were varied between their minimum and
291 maximum values (Table 1) resulted in ice volume changes of -43.2% to +41.2% (Fig. 3) from their defaults across all domains.
292 Minimum S parameter values reduced basal velocities by a mean of -24.4% across all domains (-79.5% in the Copiapó
293 domain), resulting in thicker ice (mean: +15.5%). Conversely, maximum values increased basal velocities by a mean of +47.7%
294 (+235% in the Copiapó domain), leading to thinner ice with a mean of -17.3%. The larger percentage volume changes of the
295 Copiapó domain reflect its low ice cover as small changes to the already small volume of ice (1.1 km³) yields large relative
296 differences.



297
 298 **Figure 6: Example of the influence of sliding component parameters on basal ice velocity in the Kaka & Boopi (#3) domain**
 299 (*Ancohuma Ice Caps*). Additional examples are provided in the Supplementary Information. Increased parameter values enhance
 300 basal velocities, while decreased values reduce them. Variations amplify or suppress sliding patterns already present in the default
 301 simulation. ‘Max’ and ‘min’ parameter values are listed in [Table 1](#).

302 Collectively varying all parameters of the E, T, and S components between default, minimum, and maximum values ([Table 1](#))
 303 produced a maximum mean ice volume increase of +109.3% across all five domains (Santa domain max: +247.2%), driven by
 304 the {E_min, T_max, S_min} combination ([Fig. 3](#)). The second highest mean increase of +89.3% (Santa domain max: +221.3%)
 305 resulted from {E_default, T_max, S_min}. Averaging across all combinations that include T_max or T_min produced mean
 306 ice volume changes of +33.6% and -22.6%, respectively, while those that include S_max or S_min produced changes of
 307 +38.6% and -23.2% respectively. Pearson correlation analysis ([Table 4](#)) confirms a strong and significant correlations
 308 ($p \leq 0.05$) for the T and S components and their effects on simulated ice volume in almost all domains.

309 **Table 4: Pearson correlation statistics for all domains (n = 27 simulations per domain, 135 simulations overall) to**
 310 **understand the impact of model components on simulated ice volume. A value closer to zero (0) indicates a lower**
 311 **influence on the simulated volume output. A positive or negative number indicates that when the component value is**
 312 **varied it causes a gain or loss of simulated ice volume. These are then averaged, using their absolute values to show the**
 313 **overall influence across all domains. * = $p \leq 0.05$, ** = $p \leq 0.01$.**

| Domain | E | T | S |
|---------------------|--------|--------|--------|
| Pearson correlation | Volume | Volume | Volume |



| | | | |
|------------------------|-------|---------|--------|
| Santa | -0.16 | 0.47* | -0.39* |
| Vilcanota | -0.18 | -0.36 | 0.51 |
| Kaka & Boopi | -0.17 | 0.47* | -0.46* |
| Copiapó | -0.17 | -0.46* | 0.47* |
| Mendoza, Maipo & Rapel | -0.13 | -0.49** | 0.45* |
| <i>Average</i> | 0.16 | 0.45 | 0.46 |

314 Given its limited influence on simulated ice volume, the enhancement factors (E) with E_{SIA} and E_{SSA} parameters, is excluded
315 from the individual parameter sensitivity analysis of Stage 2. The subglacial (T) and sliding (S) components demonstrated
316 significant impacts through both univariate and multivariate perturbations and were included in the Stage 2 sensitivity
317 experiments (Sect. 4.2).

318

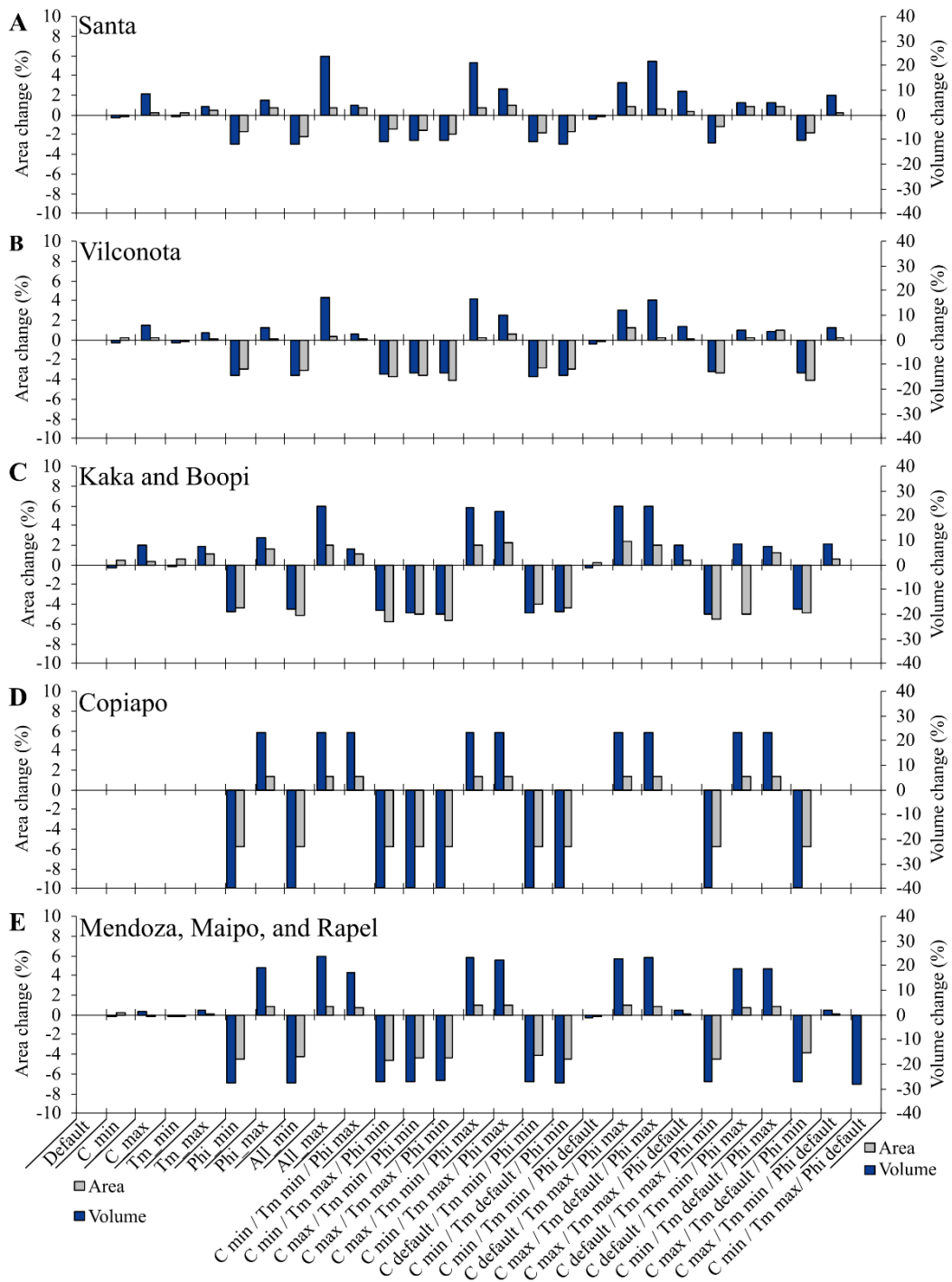
319 **4.2 Stage 2 – Individual parameter sensitivity analysis**

320 **4.2.1 Subglacial model parameters (T Component)**

321 The T component parameter tests investigated the subglacial water decay rate (C), the maximum thickness of subglacial water
322 (W_{till}^{max}), and basal friction angle (ϕ). Summary statistics for the T component tests are presented in Table 5 and Fig. 7. Among
323 all domains when the parameters were varied, the Copiapó domain, being the smallest, exhibited the largest change in simulated
324 ice volume (-40.5%). The second largest change (+28.3%) occurred in the Mendoza, Maipo and Rapel domain, the largest and
325 most ice-rich domain.

326 **Table 5: Overall, subglacial sensitivity analysis outputs detailing the default model simulation volume, and the maximum absolute**
327 **percentage changes for volume for each domain across all the model simulation when components were varied between their**
328 **maximum and minimum values.**

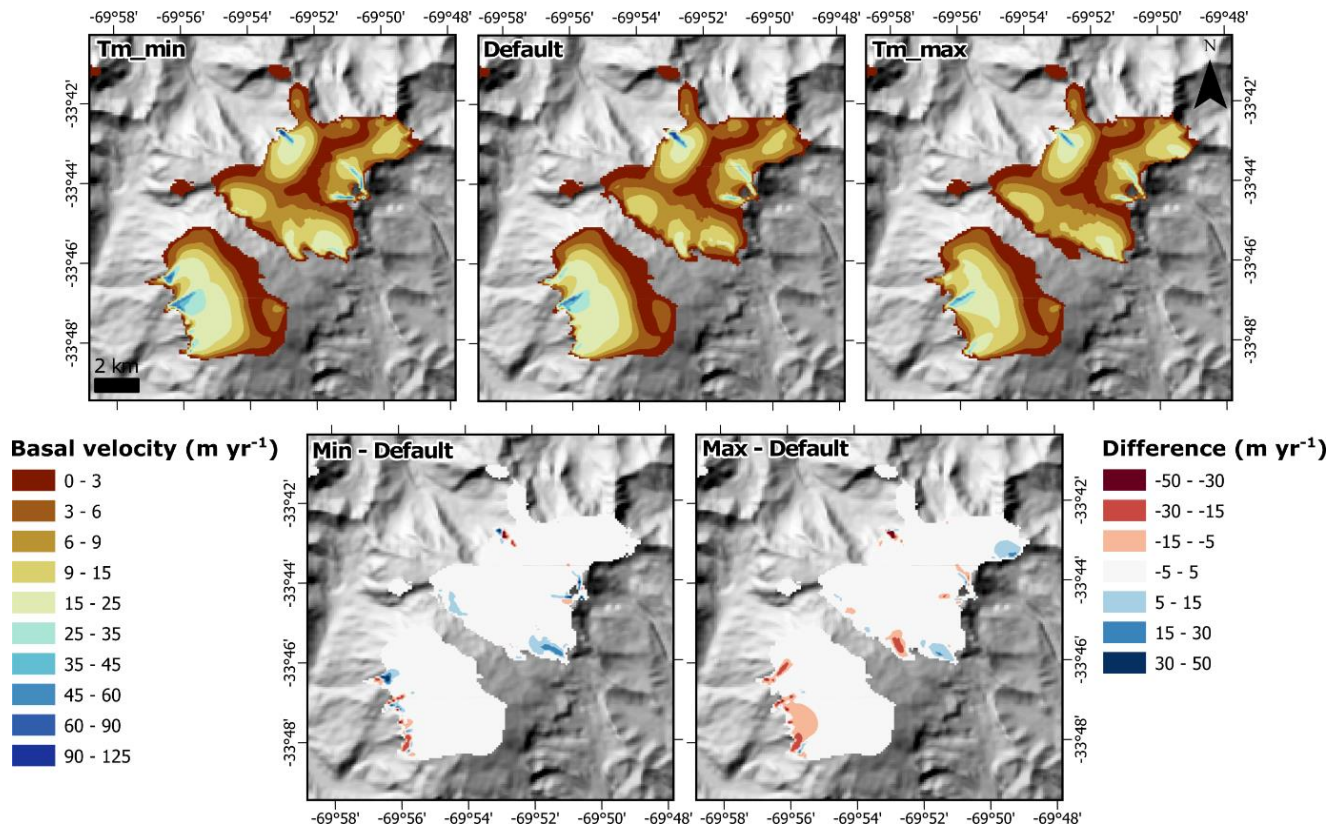
| Domain | Volume (km ³) | | | | Max abs change (%) |
|------------------------|---------------------------|------|------|--|-----------------------|
| | Default | Max | Min | | |
| Santa | 10.1 | 12.5 | 8.95 | | 23.6 |
| Vilcanota | 3.1 | 3.6 | 2.6 | | 17.2 |
| Kaka & Boopi | 2.2 | 2.7 | 1.8 | | 23.6 |
| Copiapó | 1.1 | 1.4 | 0.7 | | 40.5 |
| Mendoza, Maipo & Rapel | 17.6 | 21.8 | 12.6 | | 28.3 |





334 Varying the subglacial water decay rate (C) between its minimum and maximum values (Table 1) resulted in ice volume
 335 changes of -1.4% to +8.6% respectively across most domains. No change was observed in the Copiapó domain, likely due the
 336 small size of its glacial ice, or due to PISMs simplified hydrology model not able to affect the small glaciers due to the model
 337 resolution. Ice thickness and basal velocity changes across all domains were minor or negligible (e.g., no change in the Copiapó
 338 domain, Fig. SI 25). Minimum C values slightly reduced ice thicknesses (mean: -1.0%) and increased velocities (mean: +1.6%,
 339 -7.5% in the Vilcanota domain). Maximum C values increased thickness (mean: +5.1%) and decreased velocities (mean: -
 340 14.6%), reflecting the larger deviation of the maximum (12 mm/a) from the default (1 mm/a) relative to the minimum (0.1
 341 mm/a).

342 When W_{till}^{max} was varied between its minimum and maximum values (Table 1), it resulted in ice volume changes of between -
 343 1.0% to +7.7% across all domains (Fig. 7). No changes were seen across the Copiapo domain. Minimum W_{till}^{max} saw minimal
 344 reductions in ice thickness (mean: -0.2%) and increases in velocity changes (mean: +3.3%), while maximum W_{till}^{max} provided
 345 slightly increased ice thickness (mean: +2.5%) and reduced ice velocity (-6.6%) across all domains (Fig. 8). A stronger
 346 reduction of -13.1% in ice velocity was identified in the Vilcanota domain with minimum W_{till}^{max} values, inferred to be related
 347 to the domain geometry or resolution effects within this region.





349 **Figure 8: An example of the influence of the W_{till}^{max} (Tm in Fig. panels) parameter on the output of ice basal velocity in the Mendoza,**

350 Maipo, and Rapel (#5) domain (Volcán Marmolejo). Remaining examples are shown in the Supplementary Information. Increased

351 values the Tm parameter generally sees no, or very little changes in basal ice velocities. Values that correspond to ‘max’ and ‘min’

352 parameter values are found in [Table 1](#).

353 The parameters W_{till}^{max} and C had minimal, to no, impact on simulated ice outputs across all domains ([Fig. 7](#)). Similar minor

354 effects of W_{till}^{max} over other valley glacier modelling efforts were reported by Candaş et al. (2020) and Žebre et al., (2021),

355 although they saw greater sensitivity in their output than in our study due to W_{till}^{max} being varied in conjunction with the till

356 effective fraction overburden (δ). No PISM-based studies to our knowledge have assessed sensitivity to C for valley glaciers.

357 However, C has been shown to have an increased influence over ice sheets settings. Albrecht et al. (2020) details that increasing

358 C from 1 to 10 mm yr⁻¹ can cause PISM to simulate an additional 11 m sea level equivalent (SLE) of meltwater from the

359 Antarctic Ice Sheet over multiple glacial cycle timescales. This increasing influence over ice sheets is likely due to the greater

360 role of subglacial hydrology in driving glacial motion and ice streaming (Kazmierczak et al., 2022; Verjans and Robel, 2024).

361 While subglacial hydrology does affect valley glaciers (Mair et al., 2002), they can effect glacier motion on diurnal time scales

362 (Nienow et al., 2005) which would make modelling their interaction difficult.. Our results indicate limited impact from these

363 specific parameters in PISM, that are likely due to either, an insufficient model resolution, the basal topography not being

364 sufficient to majorly affect basal sliding, or that the PISM hydrology is too simplistic to accurately represent its effect over

365 mountain glaciers. Neither parameter significantly affected valley glacier simulations in our PISM ensemble. These parameters

366 can likely be excluded from future valley glacier sensitivity analyses.

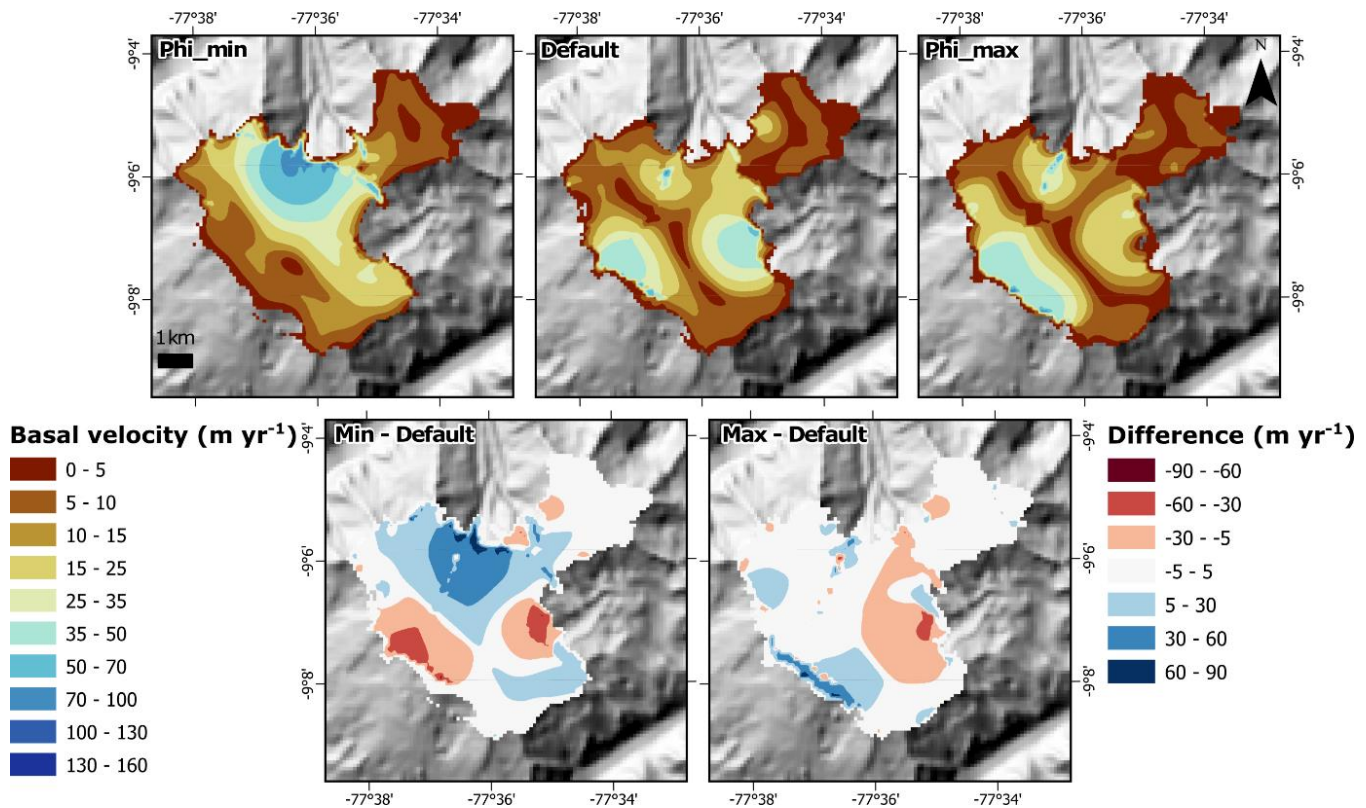
367 When ϕ was varied between its minimum and maximum values ([Table 1](#)), simulated ice volumes were saw changes between

368 -40.5% to +23.4% across the domains, respectively. Minimum values of ϕ led to substantial reductions in ice thickness (mean:

369 -24.5%) due to increases in ice velocity (mean: +81.9%), while maximum ϕ values led to increases in ice thickness (mean:

370 +19.3%) and reductions in ice velocities (mean: -23.3%) ([Fig. 9](#)). The most extreme differences were seen in the Copiapo

371 domain, due to the region incurring the smallest glacier area, and any changes can lead to larger relative (%) changes.



372

373 **Figure 9: An example of the influence of the ϕ (Phi in Fig. panels) parameter on the output of ice basal velocity in the Santa (#1)
 374 domain (Huascaran Ice Cap). Remaining examples are shown in the Supplementary Information. Increased values of the ϕ
 375 parameter see a reduction in basal velocities, while the opposite is seen for decreased values. Values of 'max' and 'min' parameter
 376 values are in Table 1.**

377 Among the T component parameters, ϕ accounted for the greatest variance in simulated ice volume (Table 7), with a consistent
 378 influence across all domains (Fig. 7). Due to ϕ representing how resistant the subglacial sediment is to shear deformation,
 379 lower values represent wet fine sandy sediments promoting more basal motion, while high values represent coarser dry gravels,
 380 or bedrock, reducing basal motion. This therefore led to decreased subglacial sliding, with higher values of ϕ leading to thicker
 381 ice (see *Phi_max* in Fig. 9), while lower values of ϕ increasing basal velocities leading to thinner ice (see *Phi_min* in Fig. 9).
 382 These influences over the ice basal velocities also yielded changes in the ice divides and flow regimes that can lead to
 383 subsequent changes in the ice thicknesses and ice velocity dynamics across the domain (see *Min - Default* in Fig 9). While ϕ
 384 has not been explicitly varied in previous valley glacier studies, to our knowledge, when modelling ice sheets ϕ is a key control
 385 on ice volume and subsequent ice dynamics (Albrecht et al., 2020; Koldtoft et al., 2021; Lowry et al., 2020). For example,
 386 lower ϕ values saw a reduction in modelled LGM volumes of the Antarctic Ice Sheet leading to accelerated retreat, whereas
 387 higher ϕ values tended to overestimate present-day ice sheet thicknesses (Albrecht et al., 2020; Lowry et al., 2020). Our
 388 findings highlight its importance in mountain glacier settings. Though a uniform ϕ was used here, it likely varies with



389 catchment-specific geology (Bareither et al., 2008; Clarke, 2018), suggesting future studies should tune ϕ regionally to improve
390 accuracy in ice dynamics and volume simulations.

391 When all T component parameters were varied between their minimum, default, and maximum values, simulated ice volume
392 differed by up to +40.5% relative to the default simulation s. Across all domains, ice volumes cluster into three distinct groups
393 centered on the minimum, default, and maximum ϕ values, most clearly seen in the Copiapó (#4) and the Mendoza, Maipo
394 and Rapel (#5) domains (Fig. 7). While ϕ exerts dominant control over ice volumes, C and W_{till}^{max} cause only minor variations
395 within these groups. The highest volumes occurred when ϕ and other subglacial parameters were set to their maximum values
396 {All_max}. Pearson correlations (Table 6) confirm the strong overwhelming influence of ϕ on simulated ice outputs, with an
397 average coefficient of 0.94 across all domains. Moreover, ϕ was the only subglacial parameter with a
398 statistically significant effect ($p \leq 0.01$), underscoring its primary role in controlling
399 model outputs in PISM.

400 **Table 6: Pearson correlation statistics for all five model domains (n = 27 simulations per domain; 135 total) showing the influence**
401 **of subglacial model parameters on simulated ice volume. Explanation of Pearson correlation values shown in Table 4. ** = p ≤ 0.01.**

| Pearson correlation | Domain | C | W_{till}^{max} | ϕ |
|---------------------|------------------------|--------|------------------|--------|
| | | Volume | Volume | Volume |
| | Santa | 0.36 | 0.11 | 0.88** |
| | Vilcanota | 0.26 | 0.12 | 0.93** |
| | Kaka & Boopi | 0.18 | 0.12 | 0.95** |
| | Copiapó | 0.00 | 0.00 | 1.00** |
| | Mendoza, Maipo & Rapel | 0.09 | -0.04 | 0.96** |
| | Average | 0.18 | 0.08 | 0.94 |

402 Across both univariate and multivariate parameter tests, ϕ consistently exerted the strongest influence on model outputs among
403 the subglacial parameters. This is due to its role in the Mohr–Coulomb criterion, which governs the pseudo-plastic sliding law
404 and modulates basal resistance (Cuffey and Paterson, 2010). Higher ϕ values increase basal resistance, slowing ice flow and
405 leading to thicker ice, thereby raising total ice volume while having limited effect on ice extent. This relationship is reinforced
406 by the ‘all max’ scenario, which produced the thickest and highest volume ice across nearly all domains.

407

408 4.2.2 Sliding model parameters (S Component)

409 The S component tests focus on two parameters: the sliding exponent (q) and the velocity threshold ($U_{threshold}$). Summary
410 statistics for these tests are presented in Table 7 and Fig. 10. The PISM domains of Copiapó and Mendoza, Maipo and Rapel,
411 representing the smallest and largest glaciers respectively, display the most pronounced responses to parameter variation, with
412 maximum ice volume changes of 44.1% and 30.0%, respectively.



413
414
415

Table 7: Sliding sensitivity analysis outputs detailing the default model simulation area and volume, and the maximum absolute percentage changes for ice volume for each domain across all the simulations when components were varied between their maximum and minimum values.

| Domain | Default | Volume (km ³) | | | Max abs change (%) |
|------------------------|---------|---------------------------|------|--|-----------------------|
| | | Max | Min | | |
| Santa | 10.1 | 11.0 | 9.0 | | 11.4 |
| Vilcanota | 3.1 | 3.3 | 2.6 | | 14.9 |
| Kaka & Boopi | 2.2 | 2.6 | 1.7 | | 21.4 |
| Copiapó | 1.1 | 1.6 | 0.6 | | 44.1 |
| Mendoza, Maipo & Rapel | 17.6 | 22.5 | 12.3 | | 30.0 |

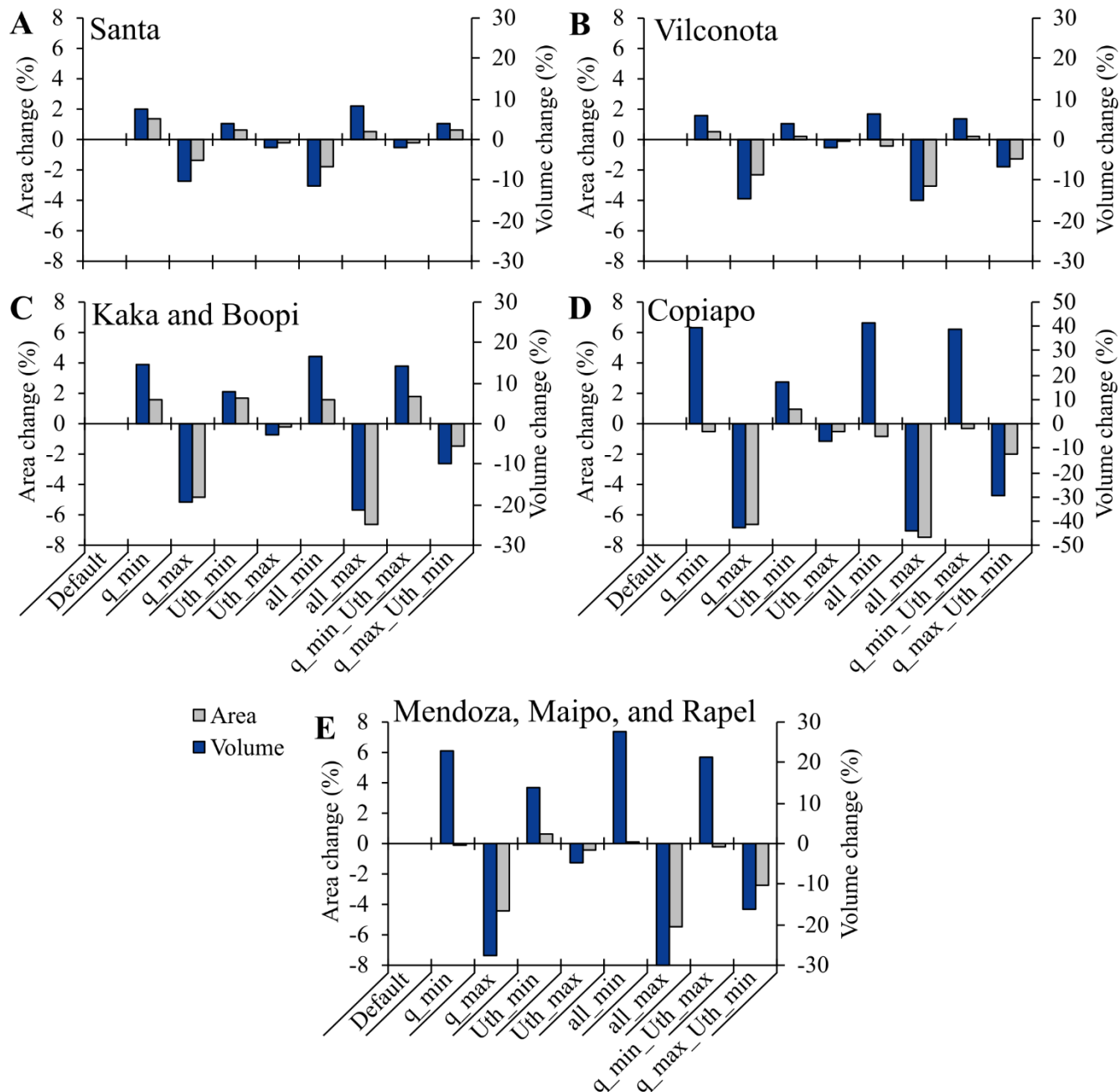
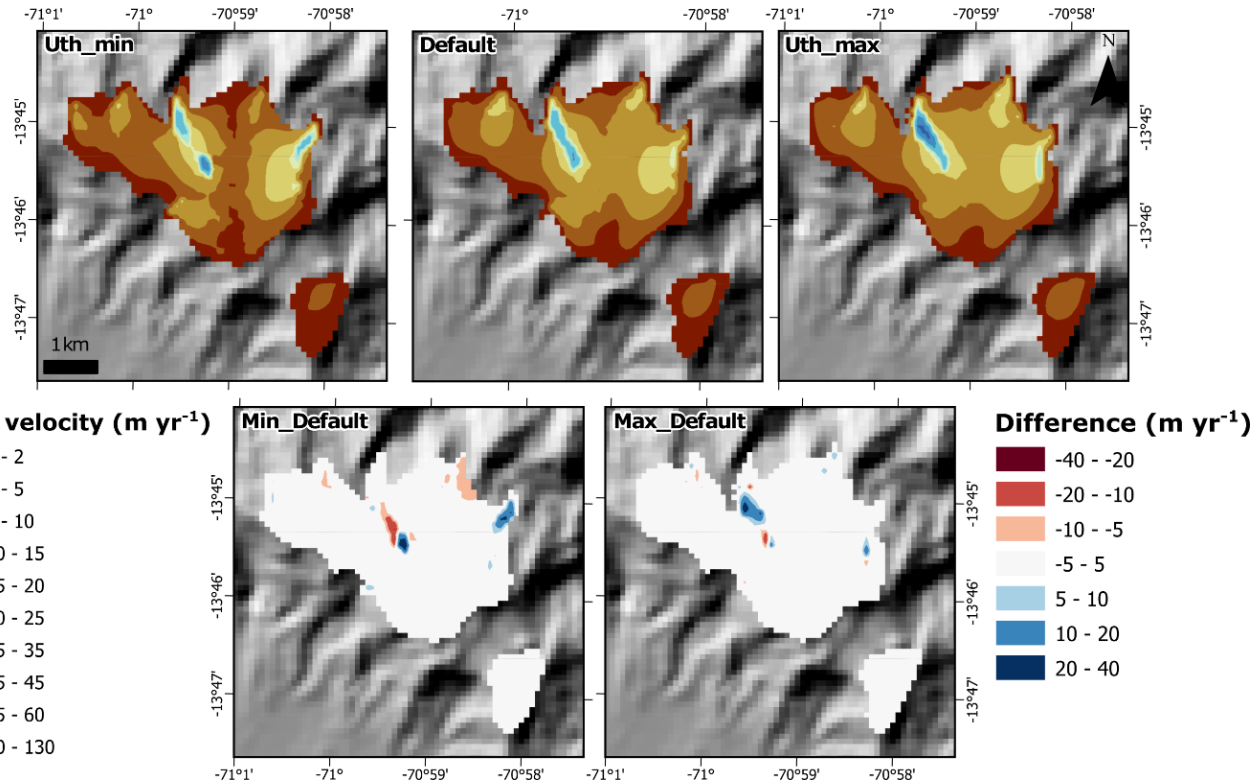


Figure 10: Sliding sensitivity analysis detailing the area (grey) and volume (blue) changes due to changing the model component parameters all together, for each of the five model domains. Blue and grey lines denote the default volume and area respectively for comparison. See Fig. 1 for domain locations. Note the change in y-axis in D), due to larger volume changes occurring in the Copiapo catchment, the catchment with the smallest ice area.

When $U_{\text{threshold}}$ was varied between its minimum and maximum values (Table 1) produced ice volume differences of +17.1% to -7.2% respectively, with an absolute average difference of 6.5%. Across all domains minimum $U_{\text{threshold}}$ saw increased ice



423 thicknesses (mean: +9.1%) and basal velocities (mean: -19.2%) (Fig. 11). Maximum $U_{threshold}$ saw reduced ice thicknesses
 424 (mean: -3.7%) along with increased basal ice velocities (mean: +7.8%).

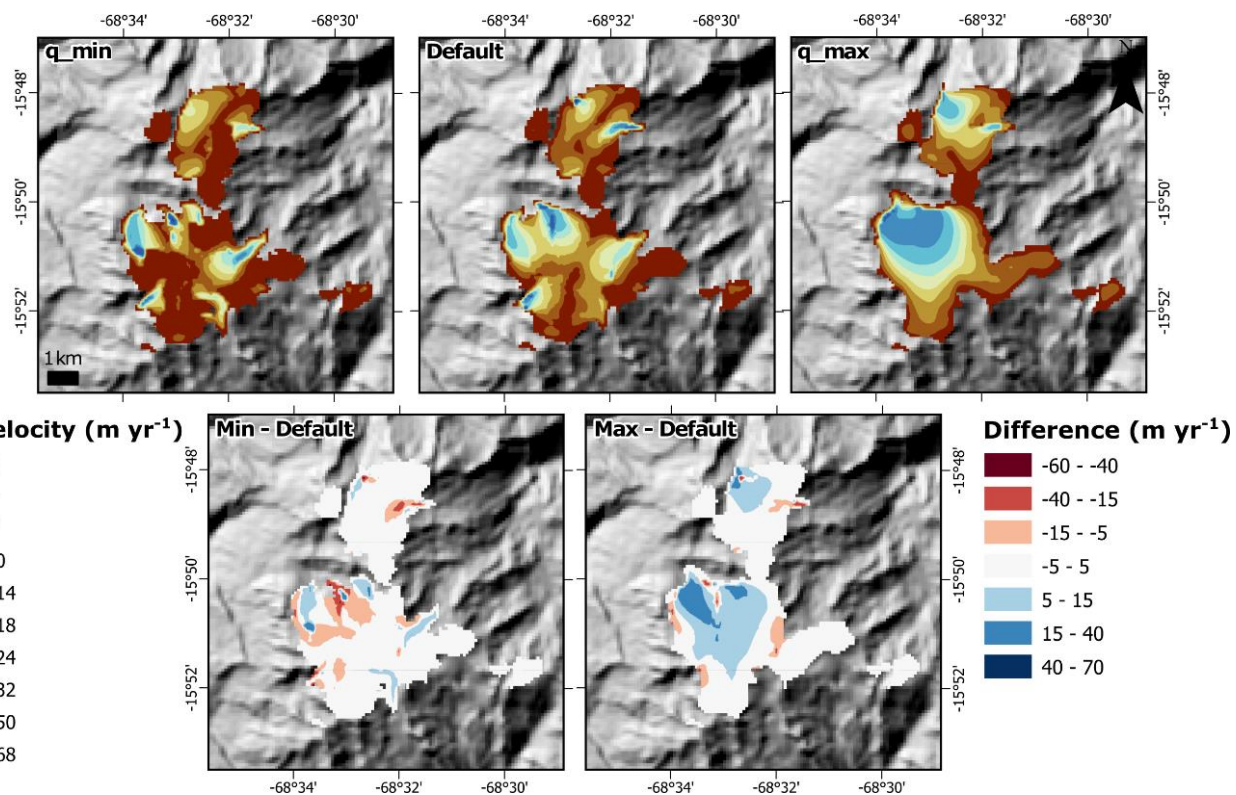


425
 426 **Figure 11: An example of the influence of the $U_{threshold}$ (U_{th} in Fig. panel) parameter on the output of ice basal velocity in the**
 427 **Vilcanota (#2) domain (Quelccaya Ice Cap). Remaining examples are shown in the Supplementary Information. An increase in the**
 428 **$U_{threshold}$ parameter sees increased basal velocities, while the opposite is seen when values are decreased. Values that correspond**
 429 **to 'max' and 'min' parameter values are found in Table 1.**

430 Variations of the $U_{threshold}$, which controls the onset of basal sliding, leads to when the $U_{threshold}$ is set to lower values, ice
 431 flow velocities are decreased, increasing ice thickness and volume. However, while overall flow patterns remain very similar,
 432 their intensity shifts with varied $U_{threshold}$ values. As can be seen in Fig. 11, with decreased $U_{threshold}$ values overall mean
 433 velocities decreased, but small localised areas of increased velocities (~ 10 to $20\ m\ yr^{-1}$) are seen where in the default run saw
 434 lower velocities occurred. When the $U_{threshold}$ is increased, overall mean velocity increased, with areas of already faster
 435 flowing ice saw an increase in velocity ($\sim 20\ m\ yr^{-1}$), with locations of localised slower velocities remaining the same as those
 436 in the default. Despite this influence, $U_{threshold}$ is rarely tested in mountain glacier modelling, with most studies using a fixed
 437 100 $m\ yr^{-1}$ value (Martin et al., 2022; Seguinot et al., 2014, 2018). Our results, spanning 20 to 200 $m\ yr^{-1}$, show that $U_{threshold}$
 438 meaningfully affects modelled dynamics and should be included in future sensitivity analyses.



439 When q was varied between its minimum and maximum values (Table 1), it produced a difference in the ice volume between
 440 +39.6% and -42.3%, with an absolute average difference of 20.4%. The two largest differences in ice volume detailed before
 441 were all seen in the smallest domain of Copiapó (-42.3%), the second highest difference is seen in Mendoza, Maipo, and Rapel
 442 domain (-27.7%), both when q is set to its maximum value. Across all domains when q was set to its minimum, there was an
 443 increase in ice thickness (mean: +18.9%) and a decrease in ice velocity (mean: -33.6%), when set to its maximum there was a
 444 decrease in ice thickness (mean: -21.7% and an increase in ice velocity (mean: +75.5%) (Fig. 12).



445

446 **Figure 12: An example of the influence of the sliding exponent (q) parameter on the output of ice basal velocity in the Kaka & Boopi**
 447 **(#3) domain (Ancohuma ice caps). Remaining examples are shown in the Supplementary Information. An increase or decrease in**
 448 **values of the q parameter see almost no effect in basal velocities. Values that correspond to 'max' and 'min' parameter values are**
 449 **found in Table 1.**

450 Variations of q within PISM exert a clear influence on simulated ice dynamics, due to its role in controlling the non-linearity
 451 of the basal sliding law (Zoet and Iverson, 2020). Higher q values suppress fast-flowing regions (e.g., $>25 \text{ m yr}^{-1}$) but enhance
 452 sliding in slower-flowing regions, producing a more diffuse velocity field (see q_{max} in Fig. 12). In contrast, lower q values
 453 concentrate flow into narrow corridors, altering ice divides and increasing ice thickness in surrounding slower-flow regions
 454 by limiting basal sliding (see q_{min} in Fig. 12). Among PISM studies, q is the most frequently varied sliding parameter,
 455 however, this is within the context of using the default Coulomb sliding model. Using the Coulomb sliding model Candaş et



456 al. (2020) over valley glaciers found that varying q altered ice volume by +22.6% at $q = 0$ and -26.4% at $q = 1$. In ice sheet
457 contexts, effects are mixed with Albrecht et al. (2020) reporting lower q reduced velocity and increased Antarctic volume at
458 the LGM by up to ± 3 m SLE. Over Greenland, Aschwanden et al. (2019) shows that the variance of q parameterization of 0.25
459 to 1.0 can lead to uncertainties on SLE contributions of 26-53% by 2100, 5-38% by 2200, and 2-33% by 2300. While the Zoet
460 and Iverson (2020) slip law has been not used by other PISM modelling studies, no study to have used the slip law within ice
461 sheet models (e.g., CISIM; van den Akker et al., 2025) varied the parameterisation of the sliding exponent extensively. Our
462 findings here support the previous conclusion that q significantly affects modelled ice volumes, particularly in regions
463 dominated by valley-confined dynamic flow (see Section 4.2.2). The results, at least for q are the first to be presented using
464 the Zoet and Iverson (2020) slip law. We therefore recommend that future valley glacier modelling studies, especially those
465 focused on mass change, include q in their sensitivity analyses.

466 When q and $U_{threshold}$ are varied together between their default, minimum, and maximum values, the largest ice volume
467 difference from the default simulation reaches -44.1%, observed in the Copiapo catchment (Fig. 10). Excluding this smallest
468 domain, the maximum difference is -30.0% in the Mendoza, Maipo and R domain. While q alone exerts the strongest influence,
469 combining both parameters amplifies their effects {All_max}. This is particularly evident when both are set to their minimum
470 or maximum values, resulting in greater or lesser increases in ice volume than when varied individually.

471 The Pearson correlation analysis (Table 8) confirms q as the dominant control on sliding-related sensitivity, with strong
472 correlations across nearly all domains except in the Santa catchment. Although the number of combined simulations is limited,
473 $U_{threshold}$ still produces noticeable changes in simulated outputs (Fig. 11), but its influence remains secondary to q when both
474 are varied simultaneously. This is likely because they both alter ice velocities, making it easier or more difficult for sliding to
475 occur. This supports that these two parameters should continue to be investigated by future model efforts over mountain
476 glaciers.

477 **Table 8: Pearson correlation statistics for all five model domains (n = 9 simulations per domain; 45 total) showing the influence of**
478 **sliding model parameters on simulated ice volume. Explanation of Pearson correlation values shown in Table 4. ** = p ≤ 0.01.**

| <i>Pearson correlation</i> | Domain | q | $U_{threshold}$ |
|----------------------------|------------------------|-----------------------|-----------------------------------|
| | | <i>Volume</i> | <i>Volume</i> |
| | Santa | 0.13 | 0.16 |
| | Vilcanota | -0.90** | -0.25 |
| | Kaka & Boopi | -0.94** | -0.24 |
| | Copiapó | -0.94** | -0.17 |
| | Mendoza, Maipo & Rapel | -0.93** | -0.24 |
| | <i>Average</i> | -0.72 | -0.15 |

479

480 4.3 Implications and recommendations for future work



481 The findings here using PISM suggest the less influential parameters mention previously can be excluded from future
482 sensitivity ensembles or parameter optimisation simulations, at least for Andean Mountain glaciers under climates close to
483 present day. This aligns with findings from other PISM-based studies in other contexts (e.g., Albrecht et al., 2020; Candaş et
484 al., 2020; Žebre et al., 2021), which similarly report minimal differences in modelled outputs when Esia, Essa, q , and C are
485 varied within reasonable bounds. Their exclusion offers the potential to streamline future modelling efforts on their parameter
486 perturbation selection, reducing computational demands and enabling more efficient ensemble designs. This enables
487 researchers to allocate computational resources toward exploring more influential parameters in greater depth or across broader
488 ranges. Further, some parameters in PISM have historically been left as ‘model defaults’ and unchanged, based on physical
489 assumptions or field data derived from non-valley glacier environments (or continental scale ice studies), limiting their
490 applicability. Additionally, many parameters have not been explored in-detail within PISM for valley glaciers which, with the
491 reduction in potential parameters to be perturbed, can now be focused on. For example, future work could examine the impact
492 of subglacial hydrology model choices, such as the difference between mass-conserving routing models and the non-
493 conserving null model used here on valley glacier dynamics.

494

495 Results from this study demonstrate that ice flow parameters influence simulated ice volume, while for ice area it is mainly
496 unaffected. For applications related to water resources, such as runoff or meltwater estimates, understanding the internal ice
497 physics and associated parameter sensitivities on ice volume is essential to understand how much ice (or water) remains in the
498 future. However, studies that focus on glacier area, or are lacking robust ice volume constraints, should prioritise sensitivity
499 analysis for climatic parameters: in particular, those using PDD models for transient simulations will likely find that climatic
500 parameters exert the strongest control over both ice area and volume.

501

502 **5 Conclusion**

503 This study investigated the influence of internal ice flow parameters within PISM over valley glaciers across our five Andean
504 domains (8 hydrological catchments) in South America. We examined parameters previously tested in smaller-scale studies,
505 and others identified as influential in different glacial environments. By applying these tests across multiple domains of varying
506 sizes, we evaluated whether sensitivity differed with glacier scale. While the smallest (Copiapó) and largest (Mendoza, Maipo
507 and Rapel) model domains, with the least and most ice respectively, exhibited the most pronounced volume differences, the
508 overall response to parameter perturbations was relatively consistent across all domains.

509 Of the components assessed, the enhancement factors showed the least sensitivity, producing the least difference in ice volume.
510 Within the subglacial component, the parameters C and W_{till}^{max} saw negligible impact on modelled ice outputs. We therefore



511 suggest that further testing of these parameters is unnecessary for similar valley glacier modelling applications in PISM,
512 especially under climate and glacier conditions close to present day.

513 The sliding component parameters of the velocity threshold ($U_{threshold}$) and sliding exponent (q), exhibited moderate influence
514 over ice volume. While both impacted ice thickness and velocity, q had the dominant influence when the sliding component
515 parameters were perturbed together. Within the till component, the greatest overall control on simulated ice volume came from
516 the till friction angle (ϕ). This saw the largest differences produced in ice thickness and basal velocities. This underscores the
517 dominant role of basal conditions in valley glacier dynamics within PISM and a parameter that should see further investigation
518 within modelling studies.

519 Unlike most previous PISM sensitivity studies, which have focused on ice sheets or limited mountain glacier domains, this
520 study systematically examined the influence of internal ice dynamics on valley glaciers in the Andes. Our findings reinforce
521 the need for detailed investigation of subglacial-related parameters, especially basal resistance (ϕ). We also detail continued
522 support for the investigation of the sliding exponent (q) within the Zoet and Iverson (2020) slip law, which was recently
523 implemented into PISM and has not been varied before this study. We also recommend that future studies explore the role of
524 subglacial hydrology models, such as the choice between mass-conserving and non-conserving schemes, and their potential
525 influence on modelled glacier behaviour, and just how this influence may be affected by model resolution.

526 This work represents the first stage in the glacier modelling workflow of the *Deplete and Retreat* project. The insights gained
527 here will directly inform the design of a Latin Hypercube ensemble by eliminating parameters with negligible impact, thereby
528 refining the efficiency and robustness of subsequent simulations. Our results can inform future sensitivity analyses and
529 optimisation studies for glacier and ice sheet models, enabling researchers to prioritise parameters with substantial impacts on
530 model outputs and avoid testing those with minimal influence. This efficiency can help conserve computational resources
531 while guiding more targeted investigations into parameter effects on modelled ice outputs.

532

533 *Supplementary Information.* Extra information on ice metrics can be found within the Supplementary Information, along with
534 extra figures that detail ice outputs from each domain. An example of the scripts used to conduct the modelling are available
535 at the DOI: [10.5281/zenodo.17878114](https://doi.org/10.5281/zenodo.17878114).

536

537 *Competing Interests.* The authors declare that they have no conflict of interest.

538



539 *Author Contributions.* JE and EL conceptualised the study. EL collated the model input data and conducted the numerical
540 modelling for the study. EL and JE analysed the model output. EL wrote the first draft. Manuscript comments and edits were
541 provided by all authors.

542

543 *Financial Support.* This work was part of the Natural Environment Research Council (NERC) highlight topic grant “Deplete
544 and Retreat: the future of Andean Water Towers” (NE/X004031/1).

545

546 *Acknowledgements.* We acknowledge the IT Services at the University of Sheffield for the provision of services for High
547 Performance Computing which was used to conduct numerical modelling in this study.

548

549 References

550 van den Akker, T., Lipscomb, W. H., Leguy, G. R., Bernales, J., Berends, C. J., van de Berg, W. J., and van de Wal, R. S.
551 W.: Present-day mass loss rates are a precursor for West Antarctic Ice Sheet collapse, *The Cryosphere*, 19, 283–301,
552 <https://doi.org/10.5194/tc-19-283-2025>, 2025.

553 Albrecht, T., Winkelmann, R., and Levermann, A.: Glacial-cycle simulations of the Antarctic Ice Sheet with the Parallel Ice
554 Sheet Model (PISM) – Part 1: Boundary conditions and climatic forcing, *The Cryosphere*, 14, 599–632,
555 <https://doi.org/10.5194/tc-14-599-2020>, 2020.

556 Archer, R.: Bayesian inference to calibrate flow geometry in ice sheet modelling of the last Scandinavian Ice Sheet,
557 University of Sheffield, 2024.

558 Aschwanden, A., Aðalgeirsdóttir, G., and Khroulev, C.: Hindcasting to measure ice sheet model sensitivity to initial states,
559 *The Cryosphere*, 7, 1083–1093, <https://doi.org/10.5194/tc-7-1083-2013>, 2013.

560 Aschwanden, A., Fahnestock, M. A., Truffer, M., Brinkerhoff, D. J., Hock, R., Khroulev, C., Mottram, R., and Khan, S. A.:
561 Contribution of the Greenland Ice Sheet to sea level over the next millennium, *Science Advances*, 5, eaav9396,
562 <https://doi.org/10.1126/sciadv.aav9396>, 2019.

563 Bareither, C., Edil, T., Benson, C., and Mickelson, D.: Geological and Physical Factors Affecting the Friction Angle of
564 Compacted Sands, *Journal of Geotechnical and Geoenvironmental Engineering*, 134, 1476–1489,
565 [https://doi.org/10.1061/\(ASCE\)1090-0241\(2008\)134:10\(1476\)](https://doi.org/10.1061/(ASCE)1090-0241(2008)134:10(1476)), 2008.

566 Berdahl, M., Leguy, G., Lipscomb, W. H., and Urban, N. M.: Statistical emulation of a perturbed basal melt ensemble of an
567 ice sheet model to better quantify Antarctic sea level rise uncertainties, *The Cryosphere*, 15, 2683–2699,
568 <https://doi.org/10.5194/tc-15-2683-2021>, 2021.



569 Bevan, S., Cornford, S., Gilbert, L., Otosaka, I., Martin, D., and Surawy-Stepney, T.: Amundsen Sea Embayment ice-sheet
570 mass-loss predictions to 2050 calibrated using observations of velocity and elevation change, *Journal of Glaciology*, 69,
571 1729–1739, <https://doi.org/10.1017/jog.2023.57>, 2023.

572 Bolibar, J., Rabatel, A., Gouttevin, I., Zekollari, H., and Galiez, C.: Nonlinear sensitivity of glacier mass balance to future
573 climate change unveiled by deep learning, *Nature Communications*, 13, 409, <https://doi.org/10.1038/s41467-022-28033-0>,
574 2022.

575 Bueler, E. and Brown, J.: Shallow shelf approximation as a “sliding law” in a thermomechanically coupled ice sheet model,
576 *Journal of Geophysical Research: Earth Surface*, 114, <https://doi.org/10.1029/2008JF001179>, 2009.

577 Buytaert, W., Moulds, S., Acosta, L., De Bièvre, B., Olmos, C., Villacis, M., Tovar, C., and Verbist, K. M. J.: Glacial melt
578 content of water use in the tropical Andes, *Environmental Research Letters*, 12, 114014, <https://doi.org/10.1088/1748-9326/aa926c>, 2017.

580 Byrne, M. P., Boos, W. R., and Hu, S.: Elevation-dependent warming: observations, models, and energetic mechanisms,
581 *Weather Clim. Dynam.*, 5, 763–777, <https://doi.org/10.5194/wcd-5-763-2024>, 2024.

582 Cai, W., McPhaden, M. J., Grimm, A. M., Rodrigues, R. R., Taschetto, A. S., Garreaud, R. D., Dewitte, B., Poveda, G.,
583 Ham, Y.-G., Santoso, A., Ng, B., Anderson, W., Wang, G., Geng, T., Jo, H.-S., Marengo, J. A., Alves, L. M., Osman, M., Li,
584 S., Wu, L., Karamperidou, C., Takahashi, K., and Vera, C.: Climate impacts of the El Niño–Southern Oscillation on South
585 America, *Nature Reviews Earth & Environment*, 1, 215–231, <https://doi.org/10.1038/s43017-020-0040-3>, 2020.

586 Calov, R. and Greve, R.: A semi-analytical solution for the positive degree-day model with stochastic temperature variations,
587 *Journal of Glaciology*, 51, 173–175, <https://doi.org/10.3189/172756505781829601>, 2005.

588 Candaş, A., Sarıkaya, M. A., KÖSE, O., Şen, Ö. L., and Çiner, A.: Modelling Last Glacial Maximum ice cap with the
589 Parallel Ice Sheet Model to infer palaeoclimate in south-west Turkey, *Journal of Quaternary Science*, 35, 935–950,
590 <https://doi.org/10.1002/jqs.3239>, 2020.

591 Carrivick, J. L., Davies, M., Wilson, R., Davies, B. J., Gribbin, T., King, O., Rabatel, A., García, J.-L., and Ely, J. C.:
592 Accelerating Glacier Area Loss Across the Andes Since the Little Ice Age, *Geophysical Research Letters*, 51,
593 e2024GL109154, <https://doi.org/10.1029/2024GL109154>, 2024.

594 Clarke, B. G.: The engineering properties of glacial tills, *Geotechnical Research*, 5, 262–277,
595 <https://doi.org/10.1680/jgere.18.00020>, 2018.

596 Cuffey, K. M. and Paterson, W. S. B.: Basal Slip, in: *The physics of glaciers*, edited by: Paterson, W. S. B., Butterworth-
597 Heinemann, London, 223–284, 2010.

598 Cuzzone, J., Romero, M., and Marcott, S. A.: Modeling the timing of Patagonian Ice Sheet retreat in the Chilean Lake
599 District from 22–10 ka, *The Cryosphere*, 18, 1381–1398, <https://doi.org/10.5194/tc-18-1381-2024>, 2024.

600 Davies, J. H.: Global map of solid Earth surface heat flow, *Geochemistry, Geophysics, Geosystems*, 14, 4608–4622,
601 <https://doi.org/10.1002/ggge.20271>, 2013.

602 Drenkhan, F., Carey, M., Huggel, C., Seidel, J., and Oré, M. T.: The changing water cycle: climatic and socioeconomic
603 drivers of water-related changes in the Andes of Peru, *WIREs Water*, 2, 715–733, <https://doi.org/10.1002/wat2.1105>, 2015.



604 Dussaillant, I., Berthier, E., Brun, F., Masiokas, M., Hugonnet, R., Favier, V., Rabatel, A., Pitte, P., and Ruiz, L.: Two
605 decades of glacier mass loss along the Andes, *Nature Geoscience*, 12, 802–808, <https://doi.org/10.1038/s41561-019-0432-5>,
606 2019.

607 Edwards, T. L., Nowicki, S., Marzeion, B., Hock, R., Goelzer, H., Seroussi, H., Jourdain, N. C., Slater, D. A., Turner, F. E.,
608 Smith, C. J., McKenna, C. M., Simon, E., Abe-Ouchi, A., Gregory, J. M., Larour, E., Lipscomb, W. H., Payne, A. J.,
609 Shepherd, A., Agosta, C., Alexander, P., Albrecht, T., Anderson, B., Asay-Davis, X., Aschwanden, A., Barthel, A., Bliss, A.,
610 Calov, R., Chambers, C., Champollion, N., Choi, Y., Cullather, R., Cuzzone, J., Dumas, C., Felikson, D., Fettweis, X.,
611 Fujita, K., Galton-Fenzi, B. K., Gladstone, R., Golledge, N. R., Greve, R., Hattermann, T., Hoffman, M. J., Humbert, A.,
612 Huss, M., Huybrechts, P., Immerzeel, W., Kleiner, T., Kraaijenbrink, P., Le clec'h, S., Lee, V., Leguy, G. R., Little, C. M.,
613 Lowry, D. P., Malles, J.-H., Martin, D. F., Maussion, F., Morlighem, M., O'Neill, J. F., Nias, I., Pattyn, F., Pelle, T., Price,
614 S. F., Quiquet, A., Radić, V., Reese, R., Rounce, D. R., Rückamp, M., Sakai, A., Shafer, C., Schlegel, N.-J., Shannon, S.,
615 Smith, R. S., Straneo, F., Sun, S., Tarasov, L., Trusel, L. D., Van Breedam, J., van de Wal, R., van den Broeke, M.,
616 Winkelmann, R., Zekollari, H., Zhao, C., Zhang, T., and Zwinger, T.: Projected land ice contributions to twenty-first-century
617 sea level rise, *Nature*, 593, 74–82, <https://doi.org/10.1038/s41586-021-03302-y>, 2021.

618 Egholm, D. L., Knudsen, M. F., Clark, C. D., and Lesemann, J. E.: Modeling the flow of glaciers in steep terrains: The
619 integrated second-order shallow ice approximation (iSOSIA), *Journal of Geophysical Research: Earth Surface*, 116,
620 <https://doi.org/10.1029/2010JF001900>, 2011.

621 Ely, J. C., Clark, C. D., Bradley, S. L., Gregoire, L., Gandy, N., Gasson, E., Veness, R. L. J., and Archer, R.: Behavioural
622 tendencies of the last British–Irish Ice Sheet revealed by data–model comparison, *Journal of Quaternary Science*,
623 <https://doi.org/10.1002/jqs.3628>, 2024.

624 Emmer, A., Le Roy, M., Sattar, A., Veetil, B. K., Alcalá-Reygosa, J., Campos, N., Malecki, J., and Cochachin, A.: Glacier
625 retreat and associated processes since the Last Glacial Maximum in the Lejjiamayu valley, Peruvian Andes, *Journal of South*
626 *American Earth Sciences*, 109, 103254, <https://doi.org/10.1016/j.jsames.2021.103254>, 2021.

627 Fick, S. E. and Hijmans, R. J.: WorldClim 2: new 1-km spatial resolution climate surfaces for global land areas, *International*
628 *Journal of Climatology*, 37, 4302–4315, <https://doi.org/10.1002/joc.5086>, 2017.

629 Flowers, G. E.: Modelling water flow under glaciers and ice sheets, *Proceedings of the Royal Society A: Mathematical,*
630 *Physical and Engineering Sciences*, 471, 20140907, <https://doi.org/10.1098/rspa.2014.0907>, 2015.

631 Fox-Kemper, B., H. T. Hewitt, C. Xiao, G. Aðalgeirsdóttir, S. S. Drijfhout, T. L. Edwards, N. R. Golledge, M. Hemer, R. E.
632 Kopp, G. Krinner, A. Mix, D. Notz, S. Nowicki, I. S. Nurhati, L. Ruiz, J. -B. Sallée, A. B.A. Slanger, and Y. Yu, 2021:
633 *Ocean, Cryosphere and Sea Level Change*, in: *Climate Change 2021 – The Physical Science Basis: Working Group I*
634 *Contribution to the Sixth Assessment Report of the Intergovernmental Panel on Climate Change*, edited by: Masson-
635 Delmotte, V., P. Zhai, A. Pirani, S. L. Connors, C. Péan, S. Berger, N. Caud, Y. Chen, L. Goldfarb, M. I. Gomis, M. Huang,
636 K. Leitzell, E. Lonnoy, J. B.R. Matthews, T. K. Maycock, T. Waterfield, O. Yelekçi, R. Yu, and B. Zhou, Cambridge
637 University Press, Cambridge, 1211–1362, 2023.

638 Fyffe, C. L., Potter, E., Fugger, S., Orr, A., Faticchi, S., Loarte, E., Medina, K., Hellström, R. Å., Bernat, M., Aubry-Wake,
639 C., Gurgiser, W., Perry, L. B., Suarez, W., Quincey, D. J., and Pellicciotti, F.: The Energy and Mass Balance of Peruvian
640 Glaciers, *Journal of Geophysical Research: Atmospheres*, 126, e2021JD034911, <https://doi.org/10.1029/2021JD034911>,
641 2021.

642 Goelzer, H., Nowicki, S., Payne, A., Larour, E., Seroussi, H., Lipscomb, W. H., Gregory, J., Abe-Ouchi, A., Shepherd, A.,
643 Simon, E., Agosta, C., Alexander, P., Aschwanden, A., Barthel, A., Calov, R., Chambers, C., Choi, Y., Cuzzone, J., Dumas,
644 C., Edwards, T., Felikson, D., Fettweis, X., Golledge, N. R., Greve, R., Humbert, A., Huybrechts, P., Le clec'h, S., Lee, V.,



645 Leguy, G., Little, C., Lowry, D. P., Morlighem, M., Nias, I., Quiquet, A., Rückamp, M., Schlegel, N. J., Slater, D. A., Smith,
646 R. S., Straneo, F., Tarasov, L., van de Wal, R., and van den Broeke, M.: The future sea-level contribution of the Greenland
647 ice sheet: a multi-model ensemble study of ISMIP6, *The Cryosphere*, 14, 3071–3096, <https://doi.org/10.5194/tc-14-3071-2020>, 2020.

649 Golledge, N. R., Mackintosh, A. N., Anderson, B. M., Buckley, K. M., Doughty, A. M., Barrell, D. J. A., Denton, G. H.,
650 Vandergoes, M. J., Andersen, B. G., and Schaefer, J. M.: Last Glacial Maximum climate in New Zealand inferred from a
651 modelled Southern Alps icefield, *Quaternary Science Reviews*, 46, 30–45, <https://doi.org/10.1016/j.quascirev.2012.05.004>,
652 2012.

653 Hardy, D. R., Vuille, M., Braun, C., Keimig, F., and Bradley, R. S.: Annual and Daily Meteorological Cycles at High
654 Altitude on a Tropical Mountain, *Bulletin of the American Meteorological Society*, 79, 1899–1914,
655 [https://doi.org/10.1175/1520-0477\(1998\)079%3C1899:AADMCA%3E2.0.CO;2](https://doi.org/10.1175/1520-0477(1998)079%3C1899:AADMCA%3E2.0.CO;2), 1998.

656 Hock, R., Bliss, A., Marzeion, B. E. N., Giesen, R. H., Hirabayashi, Y., Huss, M., Radić, V., and Slanger, A. B. A.:
657 GlacierMIP – A model intercomparison of global-scale glacier mass-balance models and projections, *Journal of Glaciology*,
658 65, 453–467, <https://doi.org/10.1017/jog.2019.22>, 2019.

659 Hoffman, A. O., Christianson, K., Holschuh, N., Case, E., Kingslake, J., and Arthern, R.: The Impact of Basal Roughness on
660 Inland Thwaites Glacier Sliding, *Geophysical Research Letters*, 49, e2021GL096564,
661 <https://doi.org/10.1029/2021GL096564>, 2022.

662 Hugonnet, R., McNabb, R., Berthier, E., Menounos, B., Nuth, C., Girod, L., Farinotti, D., Huss, M., Dussaillant, I., Brun, F.,
663 and Käab, A.: Accelerated global glacier mass loss in the early twenty-first century, *Nature*, 592, 726–731,
664 <https://doi.org/10.1038/s41586-021-03436-z>, 2021.

665 Hutter, K.: The Application of the Shallow-Ice Approximation, in: *Theoretical Glaciology: Material Science of Ice and the*
666 *Mechanics of Glaciers and Ice Sheets*, Springer Netherlands, Dordrecht, 256–332, 1983.

667 Immerzeel, W. W., Lutz, A. F., Andrade, M., Bahl, A., Biemans, H., Bolch, T., Hyde, S., Brumby, S., Davies, B. J., Elmore,
668 A. C., Emmer, A., Feng, M., Fernández, A., Haritashya, U., Kargel, J. S., Koppes, M., Kraaijenbrink, P. D. A., Kulkarni, A.
669 V., Mayewski, P. A., Nepal, S., Pacheco, P., Painter, T. H., Pellicciotti, F., Rajaram, H., Rupper, S., Sinisalo, A., Shrestha,
670 A. B., Vivioli, D., Wada, Y., Xiao, C., Yao, T., and Baillie, J. E. M.: Importance and vulnerability of the world's water
671 towers, *Nature*, 577, 364–369, <https://doi.org/10.1038/s41586-019-1822-y>, 2020.

672 Johnson, A., Aschwanden, A., Albrecht, T., and Hock, R.: Range of 21st century ice mass changes in the Filchner-Ronne
673 region of Antarctica, *Journal of Glaciology*, 69, 1203–1213, <https://doi.org/10.1017/jog.2023.10>, 2023.

674 Joughin, I., Shapero, D., and Dutrieux, P.: Responses of the Pine Island and Thwaites glaciers to melt and sliding
675 parameterizations, *The Cryosphere*, 18, 2583–2601, <https://doi.org/10.5194/tc-18-2583-2024>, 2024.

676 Kaser, G.: A review of the modern fluctuations of tropical glaciers, *Global and Planetary Change*, 22, 93–103,
677 [https://doi.org/10.1016/S0921-8181\(99\)00028-4](https://doi.org/10.1016/S0921-8181(99)00028-4), 1999.

678 Kazmierczak, E., Sun, S., Coulon, V., and Pattyn, F.: Subglacial hydrology modulates basal sliding response of the Antarctic
679 ice sheet to climate forcing, *The Cryosphere*, 16, 4537–4552, <https://doi.org/10.5194/tc-16-4537-2022>, 2022.

680 Khan, S. A., Choi, Y., Morlighem, M., Rignot, E., Helm, V., Humbert, A., Mouginot, J., Millan, R., Kjær, K. H., and Bjørk,
681 A. A.: Extensive inland thinning and speed-up of Northeast Greenland Ice Stream, *Nature*, 611, 727–732,
682 <https://doi.org/10.1038/s41586-022-05301-z>, 2022.



683 Koldtoft, I., Grinsted, A., Vinther, B. M., and Hvidberg, C. S.: Ice thickness and volume of the Renland Ice Cap, East
684 Greenland, *Journal of Glaciology*, 67, 714–726, <https://doi.org/10.1017/jog.2021.11>, 2021.

685 Koloski, J. W., Schwarz, S. D., and Tubbs, D. W.: Geotechnical Properties of Geologic Materials, in: *Engineering Geology*
686 in Washington, vol. 1, edited by: Galster, R. W., Washington Division of Geology and Earth Resources Bulletin,
687 Washiugton, 1989.

688 Lehner, B., Verdin, K., and Jarvis, A.: New Global Hydrography Derived From Spaceborne Elevation Data, *Eos, Transactions American Geophysical Union*, 89, 93–94, <https://doi.org/10.1029/2008EO100001>, 2008.

690 Lipscomb, W. H., Price, S. F., Hoffman, M. J., Leguy, G. R., Bennett, A. R., Bradley, S. L., Evans, K. J., Fyke, J. G.,
691 Kennedy, J. H., Perego, M., Ranken, D. M., Sacks, W. J., Salinger, A. G., Vargo, L. J., and Worley, P. H.: Description and
692 evaluation of the Community Ice Sheet Model (CISM) v2.1, *Geoscientific Model Development*, 12, 387–424,
693 <https://doi.org/10.5194/gmd-12-387-2019>, 2019.

694 Lliboutry, L. A. and Duval, P.: Various isotropic and anisotropic ices found in glaciers and polar ice caps and their
695 corresponding rheologies, *Annals of Geophysics*, 3, 207–224, 1985.

696 Lowry, D. P., Golledge, N. R., Bertler, N. A. N., Jones, R. S., McKay, R., and Stutz, J.: Geologic controls on ice sheet
697 sensitivity to deglacial climate forcing in the Ross Embayment, Antarctica, *Quaternary Science Advances*, 1, 100002,
698 <https://doi.org/10.1016/j.qsa.2020.100002>, 2020.

699 Maier, N., Gimbert, F., and Gillet-Chaulet, F.: Threshold response to melt drives large-scale bed weakening in Greenland,
700 *Nature*, 607, 714–720, <https://doi.org/10.1038/s41586-022-04927-3>, 2022.

701 Mair, D., Nienow, P., Sharp, M., Wohlleben, T., and Willis, I.: Influence of subglacial drainage system evolution on glacier
702 surface motion: Haut Glacier d’Arolla, Switzerland, *Journal of Geophysical Research: Solid Earth*, 107, EPM 8-1-EPM 8-13,
703 <https://doi.org/10.1029/2001JB000514>, 2002.

704 Mangeney, A. and Califano, F.: The shallow ice approximation for anisotropic ice: Formulation and limits, *Journal of
705 Geophysical Research: Solid Earth*, 103, 691–705, <https://doi.org/10.1029/97JB02539>, 1998.

706 Martin, J., Davies, B. J., Jones, R., and Thorndycraft, V.: Modelled sensitivity of Monte San Lorenzo ice cap, Patagonian
707 Andes, to past and present climate, *Frontiers in Earth Science*, 10, <https://doi.org/10.3389/feart.2022.831631>, 2022.

708 Marzeion, B., Hock, R., Anderson, B., Bliss, A., Champollion, N., Fujita, K., Huss, M., Immerzeel, W. W., Kraaijenbrink,
709 P., Malles, J.-H., Maussion, F., Radić, V., Rounce, D. R., Sakai, A., Shannon, S., van de Wal, R., and Zekollari, H.:
710 Partitioning the Uncertainty of Ensemble Projections of Global Glacier Mass Change, *Earth’s Future*, 8, e2019EF001470,
711 <https://doi.org/10.1029/2019EF001470>, 2020.

712 Masiokas, M. H., Christie, D. A., Le Quesne, C., Pitte, P., Ruiz, L., Villalba, R., Luckman, B. H., Berthier, E., Nussbaumer,
713 S. U., González-Reyes, Á., McPhee, J., and Barcaza, G.: Reconstructing the annual mass balance of the Echaurren Norte
714 glacier (Central Andes, 33.5° S) using local and regional hydroclimatic data, *The Cryosphere*, 10, 927–940,
715 <https://doi.org/10.5194/tc-10-927-2016>, 2016.

716 Masiokas, M. H., Rabatel, A., Rivera, A., Ruiz, L., Pitte, P., Ceballos, J. L., Barcaza, G., Soruco, A., Bown, F., Berthier, E.,
717 Dussaillant, I., and MacDonell, S.: A Review of the Current State and Recent Changes of the Andean Cryosphere, *Frontiers
718 in Earth Science*, 8, <https://doi.org/10.3389/feart.2020.00099>, 2020.



719 Maussion, F., Butenko, A., Champollion, N., Dusch, M., Eis, J., Fourteau, K., Gregor, P., Jarosch, A. H., Landmann, J.,
720 Oesterle, F., Recinos, B., Rothenpieler, T., Vlug, A., Wild, C. T., and Marzeion, B.: The Open Global Glacier Model
721 (OGGM) v1.1, *Geoscientific Model Development*, 12, 909–931, <https://doi.org/10.5194/gmd-12-909-2019>, 2019.

722 Millan, R., Mouginot, J., Rabatel, A., and Morlighem, M.: Ice velocity and thickness of the world's glaciers, *Nature*
723 *Geoscience*, 15, 124–129, <https://doi.org/10.1038/s41561-021-00885-z>, 2022.

724 Moreno-Parada, D., Alvarez-Solas, J., Blasco, J., Montoya, M., and Robinson, A.: Simulating the Laurentide Ice Sheet of the
725 Last Glacial Maximum, *The Cryosphere*, 17, 2139–2156, <https://doi.org/10.5194/tc-17-2139-2023>, 2023.

726 Nienow, P. W., Hubbard, A. L., Hubbard, B. P., Chandler, D. M., Mair, D. W. F., Sharp, M. J., and Willis, I. C.:
727 Hydrological controls on diurnal ice flow variability in valley glaciers, *Journal of Geophysical Research: Earth Surface*, 110,
728 <https://doi.org/10.1029/2003JF000112>, 2005.

729 Núñez Mejía, S., Villegas-Lituma, C., Crespo, P., Córdova, M., Gualán, R., Ochoa, J., Guzmán, P., Ballari, D., Chávez, A.,
730 Mendoza Paz, S., Willems, P., and Ochoa-Sánchez, A.: Downscaling precipitation and temperature in the Andes: applied
731 methods and performance—a systematic review protocol, *Environmental Evidence*, 12, 29, <https://doi.org/10.1186/s13750-023-00323-0>, 2023.

733 Payne, A. J., Nowicki, S., Abe-Ouchi, A., Agosta, C., Alexander, P., Albrecht, T., Asay-Davis, X., Aschwanden, A., Barthel,
734 A., Bracegirdle, T. J., Calov, R., Chambers, C., Choi, Y., Cullather, R., Cuzzone, J., Dumas, C., Edwards, T. L., Felikson,
735 D., Fettweis, X., Galton-Fenzi, B. K., Goelzer, H., Gladstone, R., Golledge, N. R., Gregory, J. M., Greve, R., Hattermann,
736 T., Hoffman, M. J., Humbert, A., Huybrechts, P., Jourdain, N. C., Kleiner, T., Munneke, P. K., Larour, E., Le clec'h, S., Lee,
737 V., Leguy, G., Lipscomb, W. H., Little, C. M., Lowry, D. P., Morlighem, M., Nias, I., Pattyn, F., Pelle, T., Price, S. F.,
738 Quiquet, A., Reese, R., Rückamp, M., Schlegel, N.-J., Seroussi, H., Shepherd, A., Simon, E., Slater, D., Smith, R. S.,
739 Straneo, F., Sun, S., Tarasov, L., Trusel, L. D., Van Breedam, J., van de Wal, R., van den Broeke, M., Winkelmann, R.,
740 Zhao, C., Zhang, T., and Zwinger, T.: Future Sea Level Change Under Coupled Model Intercomparison Project Phase 5 and
741 Phase 6 Scenarios From the Greenland and Antarctic Ice Sheets, *Geophysical Research Letters*, 48, e2020GL091741,
742 <https://doi.org/10.1029/2020GL091741>, 2021.

743 Pepin, N., Bradley, R. S., Diaz, H. F., Baraer, M., Caceres, E. B., Forsythe, N., Fowler, H., Greenwood, G., Hashmi, M. Z.,
744 Liu, X. D., Miller, J. R., Ning, L., Ohmura, A., Palazzi, E., Rangwala, I., Schöner, W., Severskiy, I., Shahgedanova, M.,
745 Wang, M. B., Williamson, S. N., Yang, D. Q., and Mountain Research Initiative, E. D. W. W. G.: Elevation-dependent
746 warming in mountain regions of the world, *Nature Climate Change*, 5, 424–430, <https://doi.org/10.1038/nclimate2563>, 2015.

747 Phipps, S. J., Roberts, J. L., and King, M. A.: An iterative process for efficient optimisation of parameters in geoscientific
748 models: a demonstration using the Parallel Ice Sheet Model (PISM) version 0.7.3, *Geosci. Model Dev.*, 14, 5107–5124,
749 <https://doi.org/10.5194/gmd-14-5107-2021>, 2021.

750 Pittard, M. L., Whitehouse, P. L., Bentley, M. J., and Small, D.: An ensemble of Antarctic deglacial simulations constrained
751 by geological observations, *Quaternary Science Reviews*, 298, 107800, <https://doi.org/10.1016/j.quascirev.2022.107800>,
752 2022.

753 Potter, E. R., Fyffe, C. L., Orr, A., Quincey, D. J., Ross, A. N., Rangecroft, S., Medina, K., Burns, H., Llacza, A., Jacome,
754 G., Hellström, R. Å., Castro, J., Cochachin, A., Montoya, N., Loarte, E., and Pellicciotti, F.: A future of extreme
755 precipitation and droughts in the Peruvian Andes, *npj Climate and Atmospheric Science*, 6, 96,
756 <https://doi.org/10.1038/s41612-023-00409-z>, 2023.

757 Rabatel, A., Francou, B., Soruco, A., Gomez, J., Cáceres, B., Ceballos, J. L., Basantes, R., Vuille, M., Sicart, J. E., Huggel,
758 C., Scheel, M., Lejeune, Y., Arnaud, Y., Collet, M., Condom, T., Consoli, G., Favier, V., Jomelli, V., Galarraga, R., Ginot,



759 P., Maisincho, L., Mendoza, J., Ménégoz, M., Ramirez, E., Ribstein, P., Suarez, W., Villacis, M., and Wagnon, P.: Current
760 state of glaciers in the tropical Andes: a multi-century perspective on glacier evolution and climate change, *The Cryosphere*,
761 7, 81–102, <https://doi.org/10.5194/tc-7-81-2013>, 2013.

762 Richardson, A., Carr, R., and Cook, S.: Investigating the Past, Present and Future Responses of Shallap and Zongo Glaciers,
763 Tropical Andes, to the El Niño Southern Oscillation, *Journal of Glaciology*, 1–50, <https://doi.org/10.1017/jog.2023.107>,
764 2024.

765 Roe, G. H. and Baker, M. B.: Glacier response to climate perturbations: an accurate linear geometric model, *Journal of*
766 *Glaciology*, 60, 670–684, <https://doi.org/10.3189/2014JoG14J016>, 2014.

767 Rougier, J.: Setting up your simulator, 2015.

768 Rounce, D. R., Khurana, T., Short, M. B., Hock, R., Shean, D. E., and Brinkerhoff, D. J.: Quantifying parameter uncertainty
769 in a large-scale glacier evolution model using Bayesian inference: application to High Mountain Asia, *Journal of Glaciology*,
770 66, 175–187, <https://doi.org/10.1017/jog.2019.91>, 2020.

771 Rounce, D. R., Hock, R., Maussion, F., Hugonnet, R., Kochtitzky, W., Huss, M., Berthier, E., Brinkerhoff, D., Compagno,
772 L., Copland, L., Farinotti, D., Menounos, B., and McNabb, R. W.: Global glacier change in the 21st century: Every increase
773 in temperature matters, *Science*, 379, 78–83, <https://doi.org/10.1126/science.abe1324>, 2023.

774 Schmidt, L. S., Adalgeirsdóttir, G., Pálsson, F., Langen, P. L., Guðmundsson, S., and Björnsson, H.: Dynamic simulations of
775 Vatnajökull ice cap from 1980 to 2300, *Journal of Glaciology*, 66, 97–112, <https://doi.org/10.1017/jog.2019.90>, 2020.

776 Schoof, C.: A variational approach to ice stream flow, *Journal of Fluid Mechanics*, 556, 227–251,
777 <https://doi.org/10.1017/S0022112006009591>, 2006.

778 Seguinot, J., Khroulev, C., Rogozhina, I., Stroeven, A. P., and Zhang, Q.: The effect of climate forcing on numerical
779 simulations of the Cordilleran ice sheet at the Last Glacial Maximum, *The Cryosphere*, 8, 1087–1103,
780 <https://doi.org/10.5194/tc-8-1087-2014>, 2014.

781 Seguinot, J., Ivy-Ochs, S., Jouvet, G., Huss, M., Funk, M., and Preusser, F.: Modelling last glacial cycle ice dynamics in the
782 Alps, *The Cryosphere*, 12, 3265–3285, <https://doi.org/10.5194/tc-12-3265-2018>, 2018.

783 Seroussi, H., Pelle, T., Lipscomb, W. H., Abe-Ouchi, A., Albrecht, T., Alvarez-Solas, J., Asay-Davis, X., Barre, J.-B.,
784 Berends, C. J., Bernales, J., Blasco, J., Caillet, J., Chandler, D. M., Coulon, V., Cullather, R., Dumas, C., Galton-Fenzi, B.
785 K., Garbe, J., Gillet-Chaulet, F., Gladstone, R., Goelzer, H., Golledge, N., Greve, R., Gudmundsson, G. H., Han, H. K.,
786 Hillebrand, T. R., Hoffman, M. J., Huybrechts, P., Jourdain, N. C., Klose, A. K., Langebroek, P. M., Leguy, G. R., Lowry,
787 D. P., Mathiot, P., Montoya, M., Morlighem, M., Nowicki, S., Pattyn, F., Payne, A. J., Quiquet, A., Reese, R., Robinson, A.,
788 Saraste, L., Simon, E. G., Sun, S., Twarog, J. P., Trusel, L. D., Urruty, B., Van Breedam, J., van de Wal, R. S. W., Wang, Y.,
789 Zhao, C., and Zwinger, T.: Evolution of the Antarctic Ice Sheet Over the Next Three Centuries From an ISMIP6 Model
790 Ensemble, *Earth's Future*, 12, e2024EF004561, <https://doi.org/10.1029/2024EF004561>, 2024.

791 Tadono, T., Ishida, H., Oda, F., Naito, S., Minakawa, K., and Iwamoto, H.: Precise Global DEM Generation by ALOS
792 PRISM, *ISPRS Annals of the Photogrammetry, Remote Sensing and Spatial Information Sciences*, II–4, 71–76,
793 <https://doi.org/10.5194/isprsaannals-II-4-71-2014>, 2014.

794 Talchabhadel, R., Nakagawa, H., Kawaike, K., Yamanoi, K., and Thapa, B. R.: Assessment of vertical accuracy of open
795 source 30m resolution space-borne digital elevation models, *Geomatics, Natural Hazards and Risk*, 12, 939–960,
796 <https://doi.org/10.1080/19475705.2021.1910575>, 2021.



797 Taylor, L. S., Quincey, D. J., Smith, M. W., Potter, E. R., Castro, J., and Fyffe, C. L.: Multi-Decadal Glacier Area and Mass
798 Balance Change in the Southern Peruvian Andes, *Frontiers in Earth Science*, 10, <https://doi.org/10.3389/feart.2022.863933>,
799 2022.

800 Tulaczyk, S., Kamb, W. B., and Engelhardt, H. F.: Basal mechanics of Ice Stream B, west Antarctica: 1. Till mechanics,
801 *Journal of Geophysical Research: Solid Earth*, 105, 463–481, <https://doi.org/10.1029/1999JB900329>, 2000.

802 Verjans, V. and Robel, A.: Accelerating Subglacial Hydrology for Ice Sheet Models With Deep Learning Methods,
803 *Geophysical Research Letters*, 51, e2023GL105281, <https://doi.org/10.1029/2023GL105281>, 2024.

804 Vuille, M., Francou, B., Wagnon, P., Juen, I., Kaser, G., Mark, B. G., and Bradley, R. S.: Climate change and tropical
805 Andean glaciers: Past, present and future, *Earth-Science Reviews*, 89, 79–96,
806 <https://doi.org/10.1016/j.earscirev.2008.04.002>, 2008.

807 Weertman, J.: On the Sliding of Glaciers, *Journal of Glaciology*, 3, 33–38, <https://doi.org/10.3189/S0022143000024709>,
808 1957.

809 Weis, M., Greve, R., and Hutter, K.: Theory of shallow ice shelves, *Continuum Mechanics and Thermodynamics*, 11, 15–50,
810 <https://doi.org/10.1007/s001610050102>, 1999.

811 Wilson, R., Glasser, N. F., Reynolds, J. M., Harrison, S., Anacona, P. I., Schaefer, M., and Shannon, S.: Glacial lakes of the
812 Central and Patagonian Andes, *Global and Planetary Change*, 162, 275–291,
813 <https://doi.org/10.1016/j.gloplacha.2018.01.004>, 2018.

814 Winkelmann, R., Martin, M. A., Haseloff, M., Albrecht, T., Bueler, E., Khroulev, C., and Levermann, A.: The Potsdam
815 Parallel Ice Sheet Model (PISM-PIK) – Part 1: Model description, *The Cryosphere*, 5, 715–726, <https://doi.org/10.5194/tc-5-715-2011>, 2011.

817 Wolff, I. W., Glasser, N. F., Harrison, S., Wood, J. L., and Hubbard, A.: A steady-state model reconstruction of the
818 patagonian ice sheet during the last glacial maximum, *Quaternary Science Advances*, 12, 100103,
819 <https://doi.org/10.1016/j.qsa.2023.100103>, 2023.

820 Yan, Q., Wei, T., and Zhang, Z.: Modeling the climate sensitivity of Patagonian glaciers and their responses to climatic
821 change during the global last glacial maximum, *Quaternary Science Reviews*, 288, 107582,
822 <https://doi.org/10.1016/j.quascirev.2022.107582>, 2022.

823 Yan, Q., Wei, T., and Zhang, Z.: Modeling the timing and extent of glaciations over southeastern Tibet during the last glacial
824 stage, *Palaeogeography, Palaeoclimatology, Palaeoecology*, 610, 111336, <https://doi.org/10.1016/j.palaeo.2022.111336>,
825 2023.

826 Žebre, M., Sarıkaya, M. A., Stepišnik, U., Colucci, R. R., Yıldırım, C., Çiner, A., Candaş, A., Vlahović, I., Tomljenović, B.,
827 Matoš, B., and Wilcken, K. M.: An early glacial maximum during the last glacial cycle on the northern Velebit Mt. (Croatia),
828 *Geomorphology*, 392, 107918, <https://doi.org/10.1016/j.geomorph.2021.107918>, 2021.

829 Zekollari, H., Schuster, L., Maussion, F., Hock, R., Marzeion, B., Rounce, D. R., Compagno, L., Fujita, K., Huss, M., James,
830 M., Kraaijenbrink, P. D. A., Lipscomb, W. H., Minallah, S., Oberrauch, M., Van Tricht, L., Champollion, N., Edwards, T.,
831 Farinotti, D., Immerzeel, W., Leguy, G., and Sakai, A.: Glacier preservation doubled by limiting warming to 1.5°C versus
832 2.7°C, *Science*, 388, 979–983, <https://doi.org/10.1126/science.adu4675>, 2025.



833 Zinck, A. S. P. and Grinsted, A.: Brief communication: Estimating the ice thickness of the Müller Ice Cap to support
834 selection of a drill site, *The Cryosphere*, 16, 1399–1407, <https://doi.org/10.5194/tc-16-1399-2022>, 2022.

835 Zoet, L. K. and Iverson, N. R.: A slip law for glaciers on deformable beds, *Science*, 368, 76–78,
836 <https://doi.org/10.1126/science.aazl183>, 2020.

837